FLOW VISUALIZATION STUDY OF THE INTAKE

PROCESS OF AN INTERNAL COMBUSTION ENGINE

by

Agop Ekchian

B.E. in Mechanical Engineering
American University of Beirut
(1973)

S.M. in Mechanical Engineering
Massachusetts Institute of Technology
(1976)

SUBMITTED IN PARTIAL FULFILLMENT
OF THE REQUIREMENTS FOR THE
DEGREE OF

DOCTOR OF PHILOSOPHY

at the

MASSACHUSETTS INSTITUTE OF TECHNOLOGY

(November. 1978)

Signature of Author
Department of Mechanical Engineering
November 15, 1978

Certified by....
Thesis Supervisor

Accepted by..
Chairman,
Department Committee on Graduate Students

FLOW VISUALIZATION STUDY OF THE INTAKE
PROCESS OF AN INTERNAL COMBUSTION ENGINE

by

Agop Ekchian

Submitted to the Department of Mechanical
Engineering on November 15, 1978 in partial
fulfillment of the requirements for the
Degree of Doctor of Philosophy.

ABSTRACT

The efficiency of combustion and the production
of pollutants in the internal combustion engine are
strongly dependent on the turbulent flow field in the
engine cylinder. In most engines, turbulence is almost
exclusively generated during the induction stroke. A
water analog was used to visualize and study this process
for a simple geometry cylinder.

The photographs of the flow that were obtained
confirm the expected jet type flow through the intake
valve, but demonstrate that this jet produces large
toroidal vortex structures in the cylinder for certain
operating conditions. These structures were shown to
be of the same scale as the cylinder itself and very
repeatable from cycle to cycle.

A detailed study of the characteristics of these
toroidal structures was carried out for the case of an
axisymmetric cylinder geometry. Inviscid scaling laws
were obtained from the results that describe the
development and stability of the structured flow field.
It was also observed that small changes in geometry
could have a significant effect on the induction process.

Thesis Supervisor: David P. Hoult
Title: Senior Research Associate
        Sloan Automotive Laboratory

ACKNOWLEDGEMENTS

The author would like to express his gratitute to his advisor, Dr. David P. Hoult, for his guidance and interest during the course of this work. The author also wishes to express special thanks to Prof. John B. Heywood for his valuable support throughout the author's stay at M.I.T.

The author is also grateful to Dr. Joe M. Rife and Prof. Sheila E. Widnall for serving on his thesis committee and for their frequent and helpful suggestions.

Many thanks are also due to Messers. S. J. Albano, R. R. Fenner and D. F. Fitzgerald for their assistance in the construction of the experimental equipment and their interest in the project. The author also owes a debt of gratitude to the entire faculty, staff and students of the Sloan Automotive Laboratory for making the past five years a very positive experience.

TABLE OF CONTENTS

LIST OF TABLES

LIST OF FIGURES

NOMENCLATURE

ATC   after top dead center position

BDC   bottom dead center position

C_f discharge coefficient

d_v vortex core diameter

D_o valve diameter

D_p piston diameter

D_v major diameter of vortex

L   nondimensional lift $= \dfrac{\text{valve lift}}{\text{valve dia.}}$

r   distance of a point from the closest point in vortex core (range: $o < r < d_v/2$)

R   nondimensional radius in vortex $= \dfrac{r}{R_p}$

R_p piston radius

S.A.   valve seat angle

t   time

t_c critical time for vortex breakup

u'   turbulence intensity

U   mean velocity in cylinder

V   velocity

V_p piston velocity

X_p piston displacement

δ particle diameter

Θ observed breakup angle

Θ_c predicted breakup crank angle

ν kinematic viscosity

ρ density

ω crankshaft

Ω nondimensional angular velocity in vortex

$\vec{\nabla}$ del operator

I.   Introduction

The structure of the turbulent flow field is a
determining factor in the initiation, rate of propagation,
and the efficiency of the combustion process in an
internal combustion engine. The formation of a stable
flame front, in a gasoline engine, is hampered by
fluctuations in gas velocity in the immediate vicinity
of the spark plug at the time of ignition.[1,2] This
leads to the characteristic cycle-to-cycle variations
in the cylinder peak pressure, which in turn causes
a deterioration of engine performance. On the other
hand, increasing the turbulence levels at the end of
the compression stroke enhances the lean ignition limit
and improves emissions.[3] Higher turbulence intensities
inside the combustion chamber also lead to proportionally
higher turbulent flame speeds.[4,5] This results in a
more rapid rise in the temperature and pressure of the
gas in the cylinder. These two quantities are closely
linked to pollutant emissions and to the efficiency of
combustion.

Therefore, the understanding of the turbulence in an
automotive engine is critical for the success of
present attempts to curb emissions and to improve

combustion efficiency. A great deal of effort has already been expended in an attempt to develop universal scaling laws for the turbulence in the cylinder. To date, the experimental data in support of these studies has been acquired primarily with hot-wire anemometers.

However, there are significant difficulties in using this technique to study the fluid mechanics inside an engine cylinder. The high relative turbulence intensities $\frac{u'}{U} > .2$, the highly unsteady nature of the flow, and the large pressure and temperature corrections that must be applied to hot-wire measurements (factors of 20 or more), make the results difficult to interpret. The most severe limitation of this technique, however, is that measurements can usually be obtained only at a single point in the flow field. This shortcoming is also true of the LDV (lasar doppler velocimeter) method. However, results obtained by some investigators indicate that the flow inside the cylinder may be anisotropic and nonhomogeneous, at least through the intake stroke and the early part of compression. [2,6,7]

Single point measurements of such a flow field are clearly inadequate. A complete picture of the flow structure can be obtained with the hot-wire technique

only if a matrix of measurement points covering the entire
cylinder volume is used. Results of single point
measurements are generally regarded by investigators to
be only of qualitative. value, and cannot be generalized
to apply to different combustion chamber designs. In
fact, the only universal conclusion that can be drawn
with confidence about the nature of the turbulence in
internal combustion engines is that intensity and mean
velocity are linearly dependent on engine speed.[4,8]

However, experimenters have been able to demonstrate
that, in engines without significant squish regions,
turbulence is almost exclusively generated during
induction.[6,9,10] An extensive volume of data has been
generated in the study of this critical flow process and
the consensus is that high shear flow during induction
is the source of turbulence that is present in these engines.
The high shear nature of the flow was demonstrated by using
measurements that were obtained at several different
locations in the cylinder by probes which could traverse
the cylinder volume.[6,7]

However, the difficulty in interpreting hot-wire
and LDV data has so far made it impossible to determine
the structure of the flow field. Studies have led to the

opinion that the flow during induction must be structured[4,7,8], but no reliable picture of it has yet emerged. Such a picture is vital if a realistic fluid mechanic model of the flow during induction is to be developed.

The purpose of the experiment to be discussed here was to visualize the flow during the important induction process so as to observe the structure as a whole and obtain a complete picture of the flow field. The photographs of the flow that were obtained confirm the expected jet type flow through the intake valve, but demonstrate that this jet produces large toroidal vortex structures in the cylinder for certain operating conditions. These structures were shown to be of the same scale as the cylinder itself and very repeatable from cycle to cycle.

Past experiments have shown that parameters such as valve lift, valve seat angle and the distance between the valve and the cylinder wall have an important effect on the flow through the intake valve opening.[11,12] These parameters affect the discharge coefficient of the intake valve and thus determine the maximum density of charge that can be obtained in the engine cylinder at the end of induction. This visualization experiment shows

that these quantities have a more far-reaching influence.
They not only alter the flow in the immediate vicinity
of the valve throat, but also have a signficant effect
on the entire flow field of the cylinder volume during
the whole induction process.

A water analog was used for visualization purposes
in this experiment. The study deals mainly with the
intake process in an axisymmetric cylinder with a centrally
located intake valve. This idealized case was chosen
because it was possible to identify and analyze the
important flow characteristics. Similar flow structures
were shown to exist in a more conventional geometry, but
were too complicated to be analyzed even by this
visualization technique.

Other visualization methods such as Schleiren and
shadowgraphy exist which can be used in an actual
engine; but they are not well-suited for the study of
flows, such as the intake process, where density gradients
are minimal. These methods also have the drawback that
the image obtained is integrated over a line of sight which
passes through a very complicated flow field.

However, no visualization technique can be expected
to replace LDV or hot-wire anemometry in the study of

turbulent flows. It can only be used to enhance the
understanding of results obtained by these techniques
by reducing the guesswork that is now necessary. For
example, the appreciation of the flow structure would
alleviate the directional ambiguity of the hot-wire
anemometer and also enable investigators to choose more
strategic locations for point measurements.

II. Apparatus

The mechanism that was used in this experiment is shown schematically in Fig. 1. The fluid used was distilled water and the flow was visualized in the plexiglass cylinder shown. In order to be able to photograph the flow with a minimum of distortion, it was necessary to fit the cylinder into a plexiglass box that was also filled with water.

Water was forced into the visualization cylinder by a hydraulic actuating piston via flow straighteners (Fig. 1). Water was not pulled into the plexiglass cylinder by suction so as to avoid cavitation problems that would occur at the valve throat during high speed operation.

A 3.19 in. (8.1 cm.) diameter piston was used for all the experiments, and the clearance volume of the cylinder was maintained at 3.3 in.^{3} (54 cm.^{3}). The piston stroke was varied for the different experimental cases by changing the crank radius of the crankshaft. The range of bore-to-stroke ratios chosen for these experiments (.74 to 1.35) brackets values encountered in most production and experimental engines.

The actuating cylinder was powered by a variable speed d.c. motor (3 H.P., 1750 RPM max.) via a reduction gear

and a slider crank mechanism. The coupling was designed
so that the slave piston in the plexiglass cylinder would
travel through one induction stroke each time the
mechanism was actuated. The piston had to be manually
returned to its top center position before the next
experiment.

The cylinder head was flat and was designed to
accommodate different valve locations and valve seat
angles. Details of the valve and valve seat geometry
are given in Fig. 2. The valve diameter to piston
diameter ratio of .45 is a commonly observed value in
production engines. The intake valve also remained
stationary at a preset opening during the entire induction
process.

The photographs of the flow field were taken by
means of either a Crown Graphic, 4 x 5 format, still
camera or a Red Lake Hycam movie camera (range of operation
40 to 1,000 frames/sec.). Time reference marks were obtained
on the movie film by triggering a neon timing light in
the camera at every five degrees of rotation of the engine
crankshaft. A Trump-Ross pulse generator was mounted
on the d.c. motor shaft and was used to trigger the neon
bulb.

The films used were Polaroid type 57 in the still
camera and Kodak 4X reversal and Kodak 2484 negative in
the Hycam camera. Four General Electric DMD light bulbs
were used as the light source for the experiment.

III. Experimental Procedure

A water model was used in this experiment, instead of attempting to visualize the actual gas flow in an engine cylinder, because of two basic considerations. First, by using water it is possible to greatly reduce the velocities involved in the experiment and thus significantly simplify data acquisition. Second, and perhaps the more important reason for resorting to this model, is that no appropriate tracers exist that can be used effectively with air.

This experimental model was scaled by maintaining geometric similitude and a Reynolds number, $\frac{V_p D_p}{\nu}$, equivalence based on piston velocity, V_p, and piston diameter, D_p. Since the angular velocity of the crankshaft, ω, is directly proportional to the piston velocity, the Strouhal number, $\frac{\omega D_p}{V_p}$, was automatically matched in this experiment. A more extensive discussion of the scaling of this problem is given in Appendix A.

For the kinematic viscosity, ν, in the Reynolds number calculation, the temperature of the intake air for an engine cylinder was assumed to be 150°F (66°C), while the temperature of water in the experiment was 70°F (21°C). Consequently, velocities in the model were scaled down by a factor of 17:1 from those commonly observed in reciprocating engines.

Fig. 3 is a plot of the approximate Mach number, at
the valve throat, during the intake process of a typical
production engine with dimensions similar to those of the
model. These values were calculated using incompressible
flow equations with actual valve lift profiles. However,
the reverse flow through the intake valve, that normally
occurs during the early part of induction, was neglected.

It is clear that during intake, Mach numbers at the
valve throat, the point of maximum velocity, are generally
lower than 0.3. Since this is the commonly accepted
threshold for neglecting compressibility effects, the
water model should be a valid analog of the actual flow
field. In fact, if reverse flow had been considered, the
Mach numbers at the early part of the induction stroke
would have been even lower.

For the bulk of the test conditions in this
experiment, polystyrene pellets, were used as tracers to
visualize the flow. These spherical pellets were almost
neutrally buoyant (1.01 to 1.04 specific gravity) and
ranged in diameter from .02" to .03" (0.5 mm to 0.8mm)
or from .03" to .04" (0.8 mm to 1.0 mm), depending on the
experiment. The larger pellets were used for the faster
speeds since more reflected light was necessary. For these
experimental conditions, only a single .25 in. (.63 cm)

thick plan parallel to the axis of the cylinder was illuminated at a time. Pictures of the flow were taken at 90° to this plane. A schematic of this technique is shown in Fig. 4. Of course, only the pellets that are in this illuminated zone, indicated by open circles in the figure, can reflect any light and be recorded by the camera. Since the thickness of the illuminated zone was only 8 percent of the total cylinder diameter, the photographs obtained are essentially a record of only one plane of the motion. It was necessary to study one plane at a time because of the complexity of the flow field.

The photographs obtained in this way were used to determine the structure of the flow, obtain velocity measurements, and also obtain particle trajectories.

Velocity measurements were made by measuring streak lengths left by the tracer particles on the photographic film. The lengths of these streaks, which were controlled by adjusting the exposure time of the camera, corresponded to one or two crank angle degrees of rotation of the driving crankshaft.

Particle trajectories, on the other hand, were measured by filming at high enough speeds so that particles could not travel too far between frames of the movie. Consequently, the motion of each particle could be followed

over a significant number of crank angles. Exposure times
used in these cases corresponded to approximately 0.2
crank angle degrees.

The effectiveness of using polystyrene pellets as
tracers to obtain velocity measurements has been tested
by experimenters. Allen and Yerman report an error of
only 2-4 percent, for moderate flow velocities (3-6 ft./
sec.), by comparison to pitot tube measurements.[13]
Roberson predicts a 3-8 percent deviation of the path of a
polystyrene sphere (1 mm in diameter and a specific
gravity of 1.05) from the streamlines of highly swirling
flows that are commonly observed in combustion systems.[14]
In the highly complex flow field of this experiment, however,
the error was estimated from the photographs to be
approximately 10 percent. This was accomplished by comparing
velocities, at the valve throat, measured from the
photographs with calculated values. This was sometimes
possible when particles entered the intake jet near the
valve opening where velocities are approximately known.

Accuracy of this method could be increased dramatically
by using smaller diameter polystyrene pellets.[14] However,
smaller size tracers are difficult to photograph and the
size of the particles used in these experiments could not
be reduced without a serious deterioration in the quality

of the resulting pictures.

The response time of a typical particle, used in this experiment was calculated for a step rise in fluid velocity of 15 in./sec. (typical piston velocity at high speeds). An empirical drag coefficient for a sphere undergoing an unsteady motion (see Appendix B) was used to calculate the force on the polystyrene pellets.[27] It was found that a pellet, under these conditions, would accelerate from 10 percent to 90 percent of the fluid velocity in 16 milli sec. (this corresponds to 16 crank angle degrees at 2500 scale RPM and 4 crank angle degrees at 750 scale RPM).

On the other hand, a rise time (the time it takes for the intake velocity to increase from 10 percent to 90 percent of its peak value) of .06 seconds was calculated for the velocity at the valve throat at 2500 scale RPM. This is approximately four times larger than the response time of the particle above. Consequently, the response of the tracing particle is adequate for tracing the relatively slow accelerations of the bulk flow even at the highest RPM considered.

However, these particles are too large to respond to the higher frequency turbulent eddies. In fact, Faure estimates that to adequately study turbulence, it is necessary to use significantly smaller particles (~.01 mm).[16]

Such small particles were not used here because they could not be photographed satisfactorily.

Fig. 5, a sample photograph which was obtained by this technique, shows the streaks which mark the paths of the particles. The lack of ripple in these paths is not an indication of the absence of turbulence, but reflects the inability of the particles used here to respond to the small scale oscillations. In fact, the Reynolds number of the flow based on mean piston velocity and diameter ranges from 7,500 to 25,000 for the range of RPM's considered.

Finally, in another set of tests, air bubbles introduced into the cylinder were used as tracers instead of polystyrene spheres. In these cases the entire cylinder was illuminated.

IV. Test Matrix

The test conditions in this experiment were chosen
so as to determine the fundamental properties of the
flow in an internal combustion engine. In order to
observe these properties without unnecessarily complicating
the flow, a simplified axisymmetric geometry cylinder
with a stationary intake valve was used.

Table I shows an outline of the experimental operating
conditions. Three of the parameters shown, RPM, bore-to-
stroke ratio and valve lift were studied in detail for
their effect on the flow field structure. The effects
of the valve seat angle and valve location were also
investigated, but this analysis was of a qualitative nature.

In all but the eighth test condition, the axisymmetric
cylinder geometry was used. In these cases, it was only
necessary to study one axial plane of the cylinder since
the entire flow field could be described by the revolution
of any such plane about the axis.

The effect of the Reynolds number of the intake jet,
which is proportional to piston velocity, was investigated
in the first three cases shown in Table I. This investigation
was performed at two different bore-to-stroke ratios and
three different RPM's.

Test #	RPM	Bore/Stroke	L	S.A.	Valve location
1a) Effect of RPM	750	1.35	.21	45°	axisymmetric
1b) "	750	1.06	.21	45°	"
2a) "	1500	1.35	.21	45°	"
2b) "	1500	1.06	.21	45°	"
3a) "	2500	1.35	.21	45°	"
3b) "	2500	1.06	.21	45°	"
4) Effect of Stroke	750	.74	.21	45°	"
5a) Effect of Lift	750	1.35	.07	45°	"
5b) "	750	1.06	.07	45°	"
6) Effect of Valve Angle	750	1.06	.21	60°	"
7a) "	750	1.06	.21	30°	"
7b) "	750	1.06	.07	30°	"
8) Effect of Valve Location	750	1.35	.21	45°	off-center
9) Air Bubble Technique	345	.74	.07	45°	axisymmetric

Table I: Test Matrix

A range of bore-to-stroke ratios was used in this
experiment because of the correlation that was observed
between the stability of the structured flow field and
the position of the piston in the cylinder. Test #4,
in conjunction with tests 1a and 1b, bracket the values of
bore-to-stroke ratio that are encountered in most
automotive engines.

Since a stationary valve was used in this experiment,
test #5 was performed to study the effect of the small lifts
that are encountered during the early part of induction in
actual engines. Valve lift is defined as the axial
distance moved by the valve stem from its fully closed
position. The range of dimensionless lift L (valve lift/
valve dia.) that was used here is the range of operation
commonly encountered.

The next two cases, nos. 6 & 7, were qualitative
investigations of the effect of changing the valve seat
angle (indicated as S.A. in Fig. 2).

In case #8, the experimental apparatus was fitted
with a more conventional offset intake valve. This resulted
in a much more complicated induction process, but comparisons
were possible with the simpler geometry. Because the flow
was no longer axisymmetric, two perpendicular planes
(shown in Fig. 6) were photographed.

Finally, case #9 was performed without the polystyrene tracers. In this case, air bubbles were introduced into the visualization cylinder which allowed a different aspect of the flow, its stability, to be studied. Only in this test was the entire flow field illuminated and studied as a whole.

It should be noted that each test in Table I was repeated several times. Where data from different runs of the same test condition are reported, they are differentiated by lower case Roman numerals.

V.   Results and Discussion

The photographs of the visualization of the induction
stroke in the axisymmetric cases (unless otherwise indicated,
the discussion will be restricted to the axisymmetric cases)
indicate the presence of a structured flow that is comprised
of two toroidal vortices. This flow field is shown in the
photograph in Fig. 5, while the schematic in Fig. 7
shows the ring shaped axes of rotation of the two vortices.

These two rings are formed early in the induction
stroke as the intake flow separates at the valve and
the valve seat. The upper vortex, shown in Figs. 5
and 7, is approximately located in the clearance
volume of the cylinder. It is trapped in its position
by the conical intake jet and remains constant in size
and location. The lower vortex, also shown, is a moving
vortex which fills the piston swept volume. When formed
it has a major diameter, D_V, approximately equal to the
diameter of the valve. As the piston moves through its
stroke, this vortex follows the motion of the piston at
half the speed and grows in both its major and minor
diameters.

The major diameter, D_V, of either vortex ring is
defined as the distance between the two points of

intersection of the axis of rotation of the vortex
and an axial plane of the cylinder. The minor diameter,
d_v, is the diameter of the core of the vortex and is
roughly a measure of the amount of the fluid that rotates
about one center of rotation in the axial plane. It is
difficult to determine the value of d_v of the lower
vortex from the photographs. This is especially true
for the long stroke configurations where the vortex
has an oval shape late in the stroke.

These vortices also develop azimuthal oscillatory
instabilities in their cores. This instability, in the
lower vortex, grows with time and under certain conditions
leads to a breakup of the structured flow field. This
behavior is not observed in the upper vortex.

A) Reynolds number effect on flow structure - An
increase in crankshaft speed results in an increase in
the intake jet Reynolds number and a proportional decrease
in the time taken by the induction process. Figs. 8a
and 8b are photographic comparisons of the flow field for
three different cases (1a, 2a and 3a) where the RPM and
consequently the Reynolds number are increased by a
factor of 3.5. All the photographs are taken at a
bore-to-stroke ratio, B/S, of 1.35 and a dimensionless

lift of .21. The crank angle degrees from the top dead
center position of the intake stroke are noted on the
left-hand side of each row while each column represents
data from a single RPM.

The most striking feature of these photographs,
besides the structure of the flow, is the similarity of
the flow field for the three different test conditions.
The only parameters that are changed are camera shutter
speed and RPM of the crankshaft.

The growth of the lower vortex major diameter as a
function of piston position is shown graphically in Fig. 9.
Vortex diameter and piston position are made dimensionless
by dividing by valve and piston diameters respectively.
It can be seen that D_V initially has a value approximately
equal to the valve diameter and asymptotically approaches
a value 50 percent larger. This behavior is independent of
RPM, or Reynolds number, within the scatter of the data
and is only a function of dimensionless piston displacement.

Similarly, Fig. 10 indicates the independence of the
moving vortex position, X_V, from crank speed. In fact,
if the X_V is made nondimensional by dividing by piston
displacement X_p, the figure indicates that the vortex
is always halfway between the piston position at a given

time and the position of the piston at top dead center.

Fig. 11 is a log-log plot of the nondimensional
angular velocity distribution in the lower vortex, Ω, as
a function of the nondimensional position, R, for a scale
RPM of 750. Ω, is defined as angular velocity at a
given point in the lower toroidal vortex divided by
crankshaft angular velocity, ω, while R is defined as the
shortest distance from that point to the axis of rotation
of the vortex divided by the radius of the piston R_p.
This figure shows the results of angular velocity measurements
in the lower vortex for several different crank angles.
It should be noted, however, that data presented was obtained
from two or three executions of the induction process
(indicated by lower case Roman numerals) without having
varied any of the parameters.

It can be seen in Fig. 11 that the data from
several tests and many different crank angles falls
within a narrow band about a single line defined by:

$$\Omega = \frac{2.7}{R^{1.2}} \qquad R \neq 0 \qquad\qquad [1]$$

Figs. 12 and 13 demonstrate that this behavior, which can
also be observed for the higher speeds of 1500 and 2500
RPM, is independent of Reynolds number.

From Eq. 1 it is possible to calculate a nondimensional
vorticity distribution

$$W = \frac{1}{R} \quad \frac{\partial(R^2\Omega)}{\partial R} \qquad R \neq 0 \qquad [2]$$

if it is assumed that the streamlines are concentric
circles about the axis of rotation of the vortex.

The resulting distribution

$$W = \frac{2.17}{R^{1.2}} \qquad [3]$$

is shown in Fig. 14. It can be seen from the figure,
which is applicable to all three RPM's, that the distribution
of vorticity in the lower toroidal vortex is highly peaked
at the center of rotation. In fact, it is demonstrated
in Fig. 11 that the outer regions of the vortex (within the
scatter of the data) have a velocity profile that is
similar to a free vortex distribution given by:

$$\Omega = \frac{1.25}{R^2} \qquad [4]$$

Figs. 11, 12 and 13 also show that the process is
very repeatable. At a fixed R, there is not a significant
amount of cycle-to-cycle variation in angular velocity over
many cycles. Perhaps more importantly, however, the
angular velocity at a fixed point in the vortex is also
relatively constant with time or crank angle. This

indicates that, once the vortex is formed, there is not a significant amount of dissipation in the time scale of one cycle. In fact, it is possible to show (see Appendix C) that at the BDC position the lower vortex may still retain as much as 40 percent of the total mean flow kinetic energy that entered the cylinder up to that point.

At this point, three deductions may be made about the flow field in the engine cylinder: 1) The most obvious conclusion is that the velocity distribution in the lower vortex, just like vortex diameter and vortex location, is independent of Reynolds number for the range of speeds considered. 2) The flow is not only structured, but repeatable. 3) Vortex angular velocities inside a given vortex are constant with time or crank angle. This is an indication that the velocity and consequently energy are conserved by this lower vortex.

The data presented thus far indicates that simple scaling laws can be used to describe the development (position and size of toroidal vortices) and velocity distribution in the structured flow field of this model. However, it was discovered that the lower vortex, which occupied the piston swept volume, had inherent instabilities which resulted in its breakup under certain conditions.

B) Vortex instability and breakup - One of the
operating conditions which resulted in the breakup of
the structured flow over most of the cylinder volume was
the long stroke.

The effect of changing this parameter is demonstrated
in Figs. 15a and 15b. All the pictures in these two figures
are taken at a RPM of 750 and a dimensionless valve
lift of .21, while each of the three columns represents
a different bore-to-stroke ratio. For the short and medium
strokes, the two toroidal vortices were present throughout
the entire induction process. Extending the stroke
(case 4, Table I) results in a similar flow field during
the early part of induction (Fig. 15a, left column).
However, the lower vortex begins to degenerate rapidly as
the piston passes a critical position (approximately
where the piston displacement equals the bore) and at
bottom dead center, BDC, the structure is no longer visible
(Fig. 15b, left hand column).

This instability phenomenon is observed more easily
in Figs. 16a and 16b. Here, only air bubbles were used
as tracers and the entire cylinder was illuminated. Air,
being significantly lighter than water, was forced to the
center of the rapidly spinning flow, due to centrifugal

force. Consequently, the axes of rotation of the two ring
vortices were made visible without any interference from
the rest of the flow field. The sequence of pictures 'a'
through 'h' demonstrates the shape and position of these
axes at different points in the stroke up to the point where
the lower ring is destroyed.

Azimuthal oscillations are observed along the axes
of both rings almost as soon as they are formed. While
these oscillations do not change in magnitude in the upper
vortex, they grow with time in the moving ring. When the
displacement of the piston is approximately equal to
the bore, the lower ring is seen to burst into
a totally random flow.

The development of the toroidal vortices in this
experiment and the azimuthal oscillations observed along
the cores are remarkably similar to the behavior of
unbounded ring vortices, which have been studied extensively
by many investigators (see Refs. 17 through 22).

Until this breakup occurs, however, the flow field
is the same in the long and short stroke configurations.
The similarities in vortex position and diameter for these
cases are shown in Figs. 9 and 10. Figure 17 shows that
the velocity profile still lies on the curve defined by

Eq. 1; however, in this case a factor Y is applied to Ω.

$$\Omega Y = \frac{2.7}{R^{1.2}} \qquad R \neq 0 \qquad [5]$$

Y is the length ratio of the strokes in the short and long
stroke cases (Y = .55) and compensates for the higher mean
piston velocity of the long stroke configuration.

The onset of a similar instability was observed due
to decreasing the valve lift. Figures 18a and 18b
demonstrate the effect of decreasing the lift (L = .21)
by a factor of 3. Again the flow develops in the same
manner for both conditions, but in the case of the smaller
valve opening it soon passes a critical point and
the lower ring is destroyed.

The similarity in vortex development, which can
be observed in the pictures from the two cases, is also
demonstrated in Figs. 9 and 10. The size and location of
the lower vortex is not a function of valve lift.

It was found that the velocity distribution for the
smaller valve lift, shown in Fig. 19, could again be described
by Eq. 1 if a factor Z was applied the dimensionless angular
velocity Ω

$$\Omega Z = \frac{2.7}{R^{1.2}} \qquad R \neq 0 \qquad [6]$$

This factor, which compensates for the expected increase
in flow velocity due to the decrease in valve flow area,

is equal to the effective area ratio for the two cases.
This ratio is the product of the geometric flow area and
discharge coefficient ratios for the two valve lifts.
The value of Z, which was determined experimentally to
be .58, indicated that the discharge coefficient for the
lower valve lift was approximately 70 percent larger.
Similar variations in discharge coefficient as a function
of valve lift have been observed by other experimenters.[11,23]

It should also be noted that, in an actual engine where
the valve gradually opens during the induction process,
the velocities will be closer to those observed in Fig. 19
early in the stroke and those in Fig. 11 late in the stroke.
This would probably result in a velocity distribution that
would be closer to the free vortex line shown in Fig. 11.

It is important to note that the instability in this
case occurred at a point in the cycle before the piston
displacement equaled the piston bore. Consequently, piston
position is not the only governing parameter in the lower
vortex breakup.

It was found that the instability of the lower vortex
was in fact a function of the strength (circulation) of
the lower vortex and the duration of the stroke. A

nondimensional parameter

$$K = \frac{\Gamma t}{D_v^2} \qquad [7]$$

can be defined which incorporates these two effects. In
this equation, Γ is the circulation of the vortex calculated
from the Ω vs. R curves at R = .5, while 't' is the duration
of the intake stroke. The value of R = .5 was chosen
because beyond this point the circulation did not
change significantly, and at R = .5 the vortex filled
the diameter of the cylinder.

The values of K are shown in Table II for several
of the experimental cases that were studied for the breakup
phenomenon. Each breakup crank angle, θ, shown in this
table is an average value of the observed breakup points.
These points were obtained by studying movies of several
identical runs.

The breakup of the vortex in the first experiment
in Table II occurred at approximately 174 crank angle
degrees after the start of induction. The time
for this portion of the stroke was used to determine a
critical value K_c = 48 at which point breakup occurred in
this case.

It can be deduced from Table II that structured
vortex flow persisted throughout the entire induction

RPM	STROKE	LIFT	K	Θ	Θ_c
750	1.06	.21	50*	174	174
1500	1.06	.21	50	186	174
2500	1.35	.21	37	249	236
2500	1.06	.21	50	160	174
750	.74	.21	69	128	125
750	1.35	.07	66	136	131
750	1.06	.07	90	102	97

*base condition

Table II: Observed and Predicted Crank Angle of Vortex Breakup.

process only when the value of K was less than 48.

In order to test K as a criterion for vortex breakup, a critical time, t_c, for the breakup was calculated

$$t_c = \frac{K_c D_v^2}{\Gamma} \qquad [8]$$

for each case. From these values, a predicted breakup crank angle, Θ_c, was calculated for each test condition (Table II). The close agreement between observed values of the breakup, Θ, and the predicted values, Θ_c, indicates that K, essentially a critical time ratio

$$K = K_c \frac{t}{t_c} \qquad [9]$$

is an appropriate measure of the stability of this flow field.

Consequently, any parametric change which increases the strength of the lower vortex, such as increased stroke length or decreased valve lift, will hasten the destruction of the structured flow. Simply increasing RPM also increases the circulation, but in this case the time taken by one stroke is proportionally shorter, and the critical crank angle does not change. The vortex in each experimental case has a characteristic lifetime. The structured flow can survive into the compression stroke only if the duration of the induction process is shorter than this characteristic time.

This inviscid instability is very similar to the results observed by experimenters in the study of unbounded vortex rings. In these experiments a slug of fluid was ejected from an orifice and its motion was observed as it traveled in an unbounded region. It was found that these vortices became unstable approximately five diameters (diameter of the vortex generating orifice) downstream from the point where azimuthal waviness developed in the core.[18]

In this experiment, the vortex is surrounded by rigid boundaries and it cannot travel freely as in the unbounded cases. But it was possible to calculate a self-induced velocity from the measured parameters and to determine a critical breakup time based on this theory (see Appendix D). The results showed remarkable agreement. The number of azimuthal waves that were observed in the core of the vortex in this experiment also conformed to the theory which was developed for the unbounded rings (Appendix D).

The upper, stationary vortex has not yet been discussed primarily because it represents a small portion of the flow. It also has a much less exciting history. It does not change in size or location significantly throughout the entire induction stroke. It exhibits oscillations in its

core, but does not break up. It was also difficult to
obtain a significant number of velocity measurements because
tracer particles did not migrate there in large enough
numbers. However, the measurements shown in Fig. 13
demonstrate a core structure that is similar to the larger
vortex. The fact that this vortex does not break up may
be an indication of the stabilizing effect of the intake
jet on this vortex.

The following deductions can now be made: 1) The
flow structure exhibits an inviscid instability that can
be scaled by the parameter K. 2) The dimensionless vorticity
distribution is unaffected by valve lift or stroke length
until the occurrence of breakup. 3) Instability analysis
agrees well with the existing theory for unbounded toroidal
vortices.

In the next two sections the effect of changing the
geometry of the cylinder was studied. It was found that,
although small changes could have a significant effect
on the flow field, the basic characteristics of the flow
structure were the same.

C) Effect of valve angle - In tests 6 and 7 the
valve seat angle, as defined by S.A. in Fig. 2, was
changed. The pictures in Figs. 20a and 20b indicate
that for high valve lifts (left and center

columns), the flow field is essentially unaffected by the
seat angle. However, seat angle becomes important for
case 7b, where S.A. = 30° and the lift is small (L = .07).
Under these conditions (Figs. 20a and 20b, right column),
the intake jet becomes bistable; i.e., at times, it adheres
to the cylinder head while sometimes it remains detached.
In the cases where the jet was attached to the cylinder
head, it was found that the flow structure of the lower
vortex became unstable prematurely while no upper
vortex was formed. This seems to be a further indication
that the intake jet had a stabilizing effect on the vortices
in the previous cases, because when its direction is changed,
the vortex becomes more unstable.

D) Effect of valve offset – Since conventional
engines do not have axisymmetrically located intake valves,
the model was also operated with an off-center valve to
study the effect of that change in geometry. Figures 21a
and 21b indicate that in this case the vortex is again
present, at least for part of the stroke. However, the
planes of the axes of rotation of the vortices are no
longer perpendicular to the cylinder axis but are tipped
at an angle to it. Also, with this change in geometry, the
lifetime of the vortex is shorter as in the case of the

shallower valve angle.

It should be noted also that results obtained by Willis[24] seem to indicate that the ring vortex type structures are present even in the significantly more complicated flow field of the shrouded offset intake valve. It also becomes clear that, if the geometry of the model is altered, new parameters are introduced which have to be considered for their effect on the flow structure.

E) Particle trajectories - By operating the movie camera at high enough speeds, the images of the tracer particles were captured on film without blurring. Consequently, it was possible to follow a single pellet for a signficant number of crank angles.

Figure 22 shows the simultaneous trajectories of five different particles that were obtained in this fashion for the axisymmetric case. The letters A through E represent the location of each particle and the piston face at a given crank angle. Each line represents the path of one particle. This figure indicates that the assumption, that the flow with the centrally located intake valve is axisymmetric, is accurate. Also, it is observed that the particles do not frequently enter and leave the .25 in. lighted zone or cross each other's paths.

This has to be the case if the streak method is to be relied upon to produce accurate velocity measurements.

F) Concluding remarks - Under certain conditions where the lower vortex did not break up, a significant portion of the mean flow kinetic energy that entered the cylinder through the intake valve was found to be conserved in the lower vortex. In the cases where the vortex structure was destroyed, a rapid loss of kinetic energy was observed in the mean flow. This implies that if the vortex breaks up late in the compression stroke, the stored kinetic energy of the ring vortex can significantly affect the levels of turbulence intensity long after induction is over. In certain cases in this experiment, the lower vortex was observed to break up as much as 70 crank angle degrees after the BDC of the induction stroke.

VI. Conclusions

Flow visualization has made it possible to observe
the flow field during induction as a whole instead of
concentrating on one single point in the cylinder volume.
It has been possible to isolate the important characteristics,
such as structure and stability, by concentrating on a
simplified geometry.

Results obtained here can be extended qualitatively
to actual engines. The vortex ring structure, if present
in an actual engine cylinder, could upon breakup increase
combustion rates by increasing turbulence levels in the
cylinder prior to ignition. A bistable intake jet could
cause large cycle-to-cycle variations. Ring vortices
could enhance charge stratification in stratified charge
engines by isolating pockets of incoming mixture. Small
design changes from engine to engine can have a significant
effect on engine behavior.

However, the following conclusions can be applied with
confidence only to the model in question and must await
more extensive hot-wire or LDV checks in actual engines
to ascertain their importance.

    1) Under most conditions, the flow field was structured

        throughout the entire intake stroke. This structure,

when present, was independent of Reynolds

number for the range of RPM studied.

2) Small changes in geometry could significantly

affect the flow field.

3) For the axisymmetric case: a) The vortex development,

diameter and location, scale with piston displacement;

b) Velocities in the vortices scale with flow

velocities at the valve; c) Vortex breakup is

due to an inviscid instability that scales with

K and is independent of Reynolds number.

4) Ring vortices, when intact, can conserve significant

amounts of the incoming kinetic energy of the flow.

5) When the toroidal vortices are present, the flow

is highly repeatable.

6) Ring vortices are also present in off-center valve

geometry.

7) Stability analysis agrees with existing theory

developed for unbounded ring vortices.

REFERENCES

1.   R.K. Bartan et al., "An Empirical Model for Correlating
      Cycle-by-Cycle Cylinder Gas Motion and Combustion
      Variations of a Spark Ignition Engine." Paper 710163
      presented at SAE Automotive Engineering Congress,
      Detroit, Michigan, January 1971.

2.   R.E. Winsor and D.J. Patterson, "Mixture Turbulence -
      A Key to Cyclic Combustion Variation." Paper 730086,
      SAE Transactions, 1973.

3.   T. Tanuma et al,"Ignition, Combustion and Exhaust
      Emissions of Lean Mixtures in Automotive Spark
      Ignition Engines." Paper 710159 presented at SAE
      Automotive Engineering Congress, Detroit, Michigan,
      January 1971

4.   R.J. Tabaczynski, "Turbulence and Turbulent Combustion
      in Spark-Ignition Engines." Prog. Energy Combust.
      Sci., vol. 2 (1976), pp. 143-165.

5.   N.C. Blizard and J.C. Keck, "Experimental and
      Theoretical Investigation of Turbulent Burning
      Model for Internal Combustion Engines." Paper
      740191 presented at SAE Automotive Engineering
      Congress, Detroit, Michigan, February 1974.

6.   E.S. Semenov, "Studies of Turbulent Gas Flow in
      Piston Engines." Tech. Transl. F-97 NASA, pp. 122-
      147, 1963.

7.   P.O. Witze, "Measurements of the Spatial Distribution
      and Engine Speed Dependence of Turbulent Air Motion
      in an I.C. Engine." Paper 770220 presented at SAE
      International Automotive Engineering Congress and
      Exposition, Detroit, Michigan, February 1977.

8.   D.R. Lancaster, "Effects of Engine Variables on
      Turbulence in a Spark-Ignition Engine." Paper
      760159 presented at SAE Automotive Engineering
      Congress and Exposition, Detroit, Michigan,
      February 1976.

9.   W.A. Bone and D.T.A. Townend, Flame and Combustion
     in Gases, London, 1927.

10. D.E. Fuller, "Mixture Motion in an Engine Cylinder."
     Ph.D. Thesis, March 1975, St. John's College,
     Cambridge.

11. W.J.D. Annand and G.E. Roe, Gas Flow in the Internal
     Combustion Engine, Haessner Publishing, Newfoundland,
     N.J., 1974, pp. 53-75.

12. K.Tanaka, "Airflow Through Exhaust Valve of Conical
     Seat." Proc. 3rd. Int. Cong. for App. Mechs. 1,
     pp. 287-295.

13. M. Allen and A. J. Yerman, "Neutral Density Beads
     for Flow Visualization," Symposium on Flow Visualization,
     ASME Annual Meeting, November, 1960.

14. E.C. Roberson, "The Development of a Flow Visualization
     Technique." Report of the National Gas Turbine
     Establishment, No. R. 181, Pyestock, Hants.,
     November 1955.

15. F. Odar and W.S. Hamilton, "Forces on a Sphere
     Accelerating in a Viscous Fluid." J. Fluid Mech.,
     vol. 18 (1964), pp. 302-314.

16. J. Faure, "Quelques limitations theoriques des
     procedes de visualization." La Houille Blanche,
     N°3, May, 1963.

17. T. Maxworthy, "The Strucutre and Stability of Vortex
     Rings." J. Fluid Mech., vol. 51, part 1 (1972),
     pp. 15-32.

18. T. Maxworthy, "Some Experimental Studies of Vortex
     Rings." J. Fluid Mech., vol. 81, Part 3 (1977),
     pp. 465-495.

19. J.P. Sullivan, S.E. Widnall and S. Ezekiel, "Study
     of Vortex Rings Using a Lazar Doppler Velocimeter,"
     AIAA Journal, vol. 11, No. 10, October, 1973.

20. S.E. Widnall, D.B. Bliss and C-Y. Tsai, "Instability of Short Waves on a Vortex Ring." J. Fluid Mech., vol. 66 (1974), pp. 35-48.

21. C-Y Tsai and S.E. Widnall, "The Stability of Short Waves on a Straight Vortex Filament in a Weak Externally Imposed Strain Field." J. Fluid Mech., vol. 73, part 4 (1976), pp. 721-733.

22. P.G. Saffman, "The Number of Waves on Unstable Vortex Rings," J. Fluid Mech., vol 84, part 4 (1978), pp. 625-639.

23. W.B. Wallace, "High-Output Medium-Speed Diesel Engine Air and Exhaust System Flow Losses," Proc. Instu. Mech. Engrs., 1967-68, vol. 182, part 3D.

24. D.A. Willis, W.E. Mayer and C. Birnie, Jr., "Mapping of Airflow Patterns in Engines with Induction Swirls." Paper 66093 presented at SAE Automotive Engineering Congress, Detroit, Michigan, January 1966.

25. A.P. Morse, J.H. Whitelaw and M. Yianneskis, "Turbulent Flow Measurements by Laser-Doppler Anemometry in a Motored Reciprocating Engine." Imperial College, London, unpublished.

26. P.A. Thompson, Compressible-Fluid Dynamics, McGraw-Hill, New York, 1972, pp. 137-143.

27. S.K. Karanfilian and T.J. Kotas, "Drag on a Sphere in Unsteady Motion in a Liquid at Rest." J. Fluid Mech., vol. 87, part 1 (1978), pp. 85-96.

APPENDIX A - SCALING OF THE WATER MODEL TO ENGINE INTAKE CONDITIONS

During the intake process of an internal combustion engine, air is commonly assumed to be an incompressible fluid. A criterion for compressibility can be obtained from the continuity equation:

$$\vec{\nabla} \cdot \rho\vec{V} + \frac{\partial \rho}{\partial t} = 0 \qquad\qquad [A-1]$$

This can be written in a different form by expanding the first term on the left-hand side and using the definition of the substantial derivative $\frac{D(\ )}{Dt} = u \cdot (\ ) + \frac{\partial(\ )}{\partial t}$

$$\vec{\nabla} \cdot \rho\vec{V} + \frac{\partial \rho}{\partial t} = \rho\vec{\nabla}\cdot\vec{V} + \vec{V}\cdot(\vec{\nabla}\rho) + \frac{\partial \rho}{\partial t}$$
$$= \rho\vec{\nabla}\cdot\vec{V} + \frac{D\rho}{Dt}$$

So, after simplifying further,

$$-\frac{1}{\rho}\frac{D\rho}{Dt} = \vec{\nabla}\cdot\vec{V} \qquad\qquad [A-2]$$

Consequently, $\vec{\nabla}\cdot V$ is a measure of the change in density in the flow field; and the fluid may be assumed to be incompressible if the nondimensional form of this quantity is significantly smaller than 1.

$$\vec{\nabla}^* \cdot V^* << 1 \qquad\qquad [A-3]$$

where

$$\vec{\nabla}^* = D_p\vec{\nabla}$$

$$\vec{V}^* = \frac{\vec{V}}{\bar{\bar{V}}_p}$$

For an excellent discussion of the effect of compressibility see Thompson.[26] The commonly accepted limit where compressibility can be neglected is where Mach numbers are below 0.3, such that

$$\vec{V}^* \cdot \vec{V}^* \approx .1$$

is small.

The nondimensional form of the momentum equation where the fluid can be assumed incompressible is:

$$[St] \frac{\partial \vec{V}^*}{\partial t^*} + (\vec{V}^* \cdot \vec{\nabla}^*)\vec{V}^* = -\vec{\nabla}^* P^* + [Re^{-1}]\nabla^{*2} \vec{V}^* \qquad [A-4]$$

In this equation the starred quantities are dimensionless variables defined by:

$$\nabla^{*2} = D_p^2 \nabla^2$$
$$t^* = t\omega$$
$$P^* = \frac{P + \rho gz - P_O}{\rho V_p^2}$$

where 'z' is the vertical coordinate. Because of the absence of a free surface or density gradients in this experiment the gravity term has no effect on the flow and has been absorbed into the pressure term. P_O is a typical ambient pressure.

Two parameters, Reynolds number

$$Re = \frac{\bar{V}_p D_p}{\nu}$$

and Strouhal number

$$St = \frac{\omega D_p}{\bar{V}_p}$$

appear in Eq. A-4 and must be matched in the model with actual engine conditions. However, since engine shaft speed is directly proportional to the characteristic velocity $\bar{V}_p$ that is observed in the cylinder,

$$\bar{V}_p \sim \omega S$$

geometric similitude automatically leads to a Strouhal number match.

Matching Reynolds numbers between experiment and actual engine operating conditions

$$\left(\frac{\bar{V}_p D_p}{\nu}\right)_{model} = \left(\frac{\bar{V}_p D_p}{\nu}\right)_{engine}$$

while observing the geometric restriction leads to

$$\frac{\bar{V}_p \ model}{\bar{V}_p \ engine} = \frac{\nu \ air}{\nu \ water}$$

For the conditions of this experiment this ratio was 1:17.

APPENDIX B - <u>RESPONSE TIME OF POLYSTYRENE PARTICLES</u>
<u>OF TYPICAL DIAMETER</u>

The response time of a typical polystyrene pellet,
.03 inches in diameter, to a step change in velocity of
15 inches per second was calculated. This velocity was
characteristic of the velocities that were encountered in
the cylinder in this experiment.

Because of the unsteady nature of the motion
of the polystyrene pellets under these conditions,
the effect of the 'virtual mass' and the history of the
motion had to be considered.[15] The pellet was assumed
to be spherical in shape and the drag force on it was
calculated by using

$$-F_D = \frac{1}{8} C_V \pi \delta^2 \rho |V| V + \frac{1}{6} C_A \pi \delta^3 \rho \dot{V} + \frac{1}{4} C_H \delta^2 (\pi \rho \mu)^{\frac{1}{2}} \int_o^t \frac{\dot{V}(t')}{(t-t')^{1/2}} dt'$$

where
[B-1]

F_D = drag force

δ = particle diameter

ρ = fluid density

μ = fluid viscosity

V = particle velocity relative to fluid

$\dot{V}$ = particle acceleration relative to fluid

C_V = steady state drag coefficient

C_A = virtual mass coefficent

C_H = flow history coefficent

The form of the expression was determined by Boussinesq in 1885 in a theoretical calculation where he neglected the convective terms in the momentum equation. The values of the coefficients, C_A and C_H, used in this calculation were obtained from the experimental study of the drag force on a sphere in sinusoidal motion.[15] The value of the steady state coefficient was determined from the expression given by Karanfilian and Kotas.[27]

In calculating the response time of the pellet, it was assumed that drag on the particle was the only force acting on it and Eq. B-1 was integrated numerically to obtain the velocity of the pellet as a function of time. It was found that the particle increased in speed from 10 percent to 90 percent of the fluid velocity 16 milliseconds after the step change.

Using the same equations it was found that the velocity of the polystyrene pellets that was induced by gravity was an order of magnitude lower than characteristic flow velocities. Also, the total distance traveled by these pellets due solely to the effect of gravity in the time scale of the longest experiment was ~.2 inches. Consequently, the effects of gravity on the particle is negligible.

APPENDIX C - <u>CALCULATION OF THE KINETIC ENERGY OF THE</u>
<u>VORTICES</u>

For the purpose of this calculation, the velocity
distribution in the vortex was assumed to be given by
the Ω vs. R curves, such as Fig. 11, except in the
region of the axis of rotation of the vortex. Eq. [1]
can not be used for R = 0 since at that point the velocity
would become infinite. A solid body rotation was assumed
up to R = .07 since it was observed from the data that the
velocity was an increasing function (with decreasing R)
up to this point.

With these assumptions, the energy in each vortex
was calculated from

$$(K.E.)_{vortex} = \pi^2 D_v \rho \int_o^r r[V(r)]^2 \, dr \qquad\qquad [C\text{-}1]$$

where V and r are the dimensional velocity distribution
and radial position in the vortex. The value of r' in
the equation was determined from photographs. When
the cross section of the vortex was not circular an
average of the maximum and the minimum value of the
radius was used.

The total kinetic energy flux of the mean flow
was also calculated from

$$(K.E.)_{inducted} = \frac{1}{2} \frac{\rho A_e}{\omega} \int_o^\pi [V'(\theta)]^3 d\theta \qquad\qquad [C\text{-}2]$$

where V' and A_e are the mean flow velocity and the
effective flow area of the valve. The effective
flow area is equivalent to a fraction (the discharge
coefficient C_f) of the actual valve area ($\pi L D_o^2$).

It was found that the energy contained in the
two toroidal vortices at bottom dead center was a
significant fraction of the total kinetic energy
flux during induction. This calculation was sensitive
to the value of the discharge coefficent. In these
experiments values of .6 and .8 were used for C_f and
the fraction of energy in the vortices ranged from
30 percent to 56 percent of the total inducted into
the cylinder. Consequently, if the vortices are present
at BDC they will contain a significant portion of the total
kinetic energy. It is, however, difficult to determine
an exact fraction because of the dependence on C_f which
is an unknown in this case.

It should also be noted that the energy loss due to
viscous dissipation in the lower vortex is typically
one percent of the total kinetic energy contained
in the vortex and can be neglected. Viscous dissipation
per unit volume can be determined from

$$e_v = \mu \left[\frac{\partial v_\theta}{\partial r} - \frac{v_\theta}{r} \right]^2$$

where e_V and v_θ are the viscous dissipation per unit volume and tangential velocity in the vortex respectively. In this calculation the assumption must be made that the streamlines are concentric about the axis of rotation of the vortex.

APPENDIX D - <u>CALCULATION OF THE CRITICAL TIME OF BREAKUP</u>
<u>AND THE NUMBER OF AZIMUTHAL INSTABILITY</u>
<u>WAVES IN THE CORE OF THE VORTEX</u>

It was observed by Maxworthy that after the onset
of instability in the core of a ring vortex, the ring
traveled downstream approximately five of its initial
diameters before breaking up.[18] Consequently, a
theoretical time for breakup was defined as

$$t'_c = \frac{5D_O}{U'}$$ [D-1]

where D_O is the initial vortex diameter or the diameter
of the generating mechanism and U' is the self-induced
velocity of the vortex.

A vortex ring of diameter D_V, in an unbounded fluid,
will move with a self-induced velocity of:

$$U = \frac{\Gamma}{2 \pi D_V} \left[\ln\left(\frac{8D_V}{d_{ve}}\right) - \frac{1}{4} \right]$$ [D-2]

where Γ and d_{ve} are the circulation around the axis
of rotation and the effective diameter of the core of
the vortex respectively.[22] The value of d_{ve} is a
function of the actual vortex core diameter and the
distribution of the vorticity in the core:

$$d_{ve} = d_v e^{\left(\frac{1}{4} - z\right)}$$ [D-3]

and

$$Z = \frac{4\pi^2}{r^2} \int_0^{\frac{d_v}{2}} rV^2 dr \qquad [D-4]$$

where r and V are dimensional position and velocity in the core of the vortex, respectively.

From Eq. E-2 and the velocity distribution plots it was possible to calculate a hypothetical velocity U' for this experiment. (The toroidal vortices in the cylinder do not move at this velocity, however, because they are confined). Consequently, a theoretical critical time was obtained from Eq. E-1.

For the typical case of 750 RPM (case 1a) the calculation was conducted for the vortex at the bottom dead center position and a breakup time of .33 seconds was predicted. The time for the stroke was added to this value and Eq. [7] was applied, and this predicted $K = 52$ for stability. This is in good agreement with the experimental prediction of the critical value of $K = 48$.

The number of instability waves that were observed by the bubble technique also agree well with a theoretical prediction by Saffman.[22] Using the equation for N, the number of waves

$$N \approx [0.53 + 2.43(D/_S)^{2/3}] \ [1 + \frac{0.8}{\epsilon}] \qquad [D-5]$$

where ε is defined implicitly in:

$$\varepsilon R^{\frac{1}{2}} = 50\left(\frac{D}{S}\right)^{5/6} \left[1 + 0.22\left(\frac{S}{D}\right)^{2/3}\right] \left[1.24 + \frac{2}{3}\ln\left(\frac{D}{S}\right) + \ln\left[1 + 0.22\left(\frac{S}{D}\right)^{2/3}\right] - \ln(0.47 + .63\varepsilon)\right]^{-1/2} \quad [D-6]$$

In these equations $\frac{S}{D}$ is the ratio of the length of stroke of the vortex generating mechanism and the diameter of the orifice where the vortex is generated.

From these two equations a value of N = 4 was calculated while three waves were observed for the experimental case.

FLOW
STRAIGHTENER

PLEXIGLASS
BOX

MOTOR
DRIVEN

PLEXIGLASS
CYLINDER

PISTON
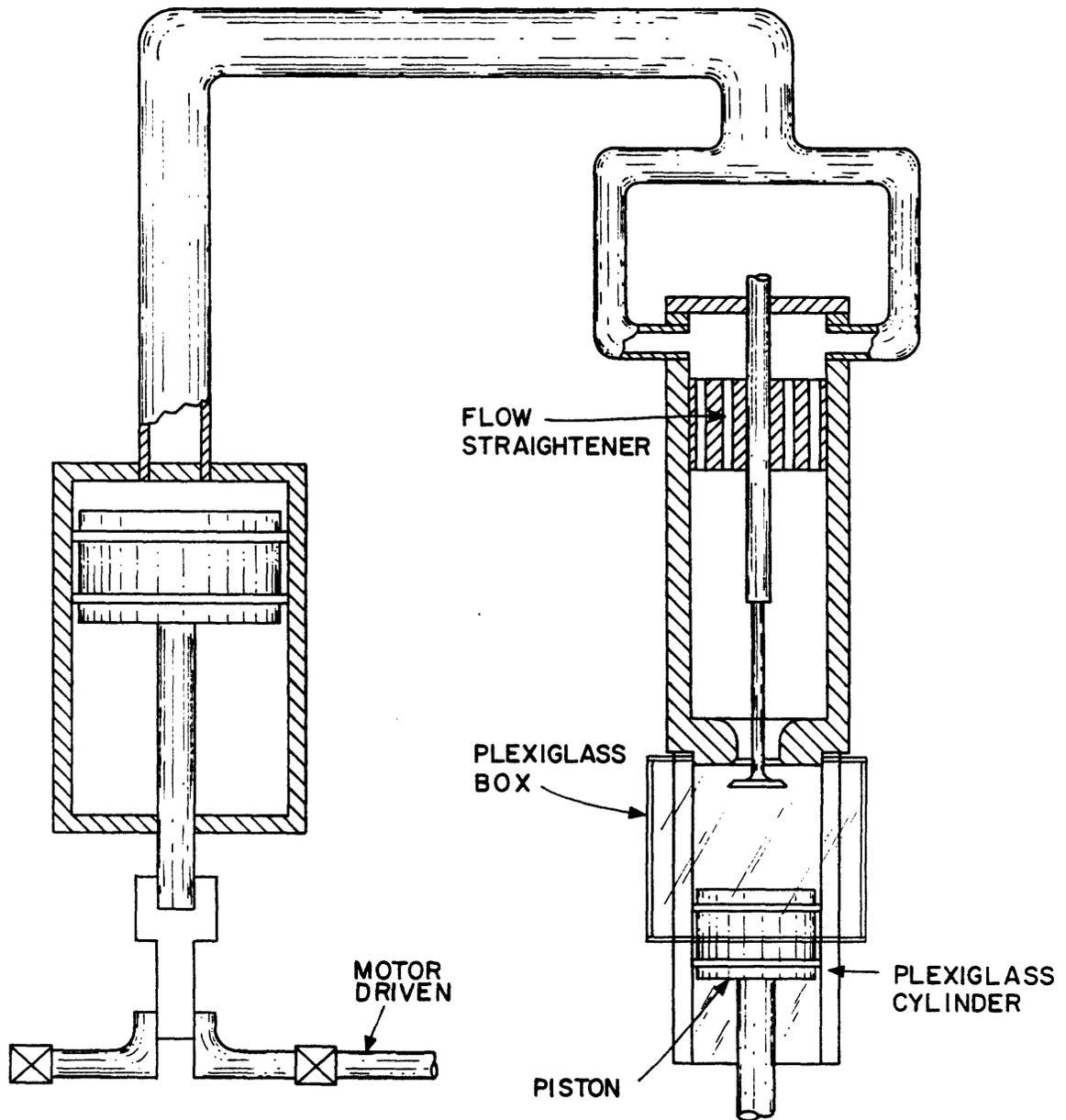
Fig. 1: Schematic of experimental apparatus
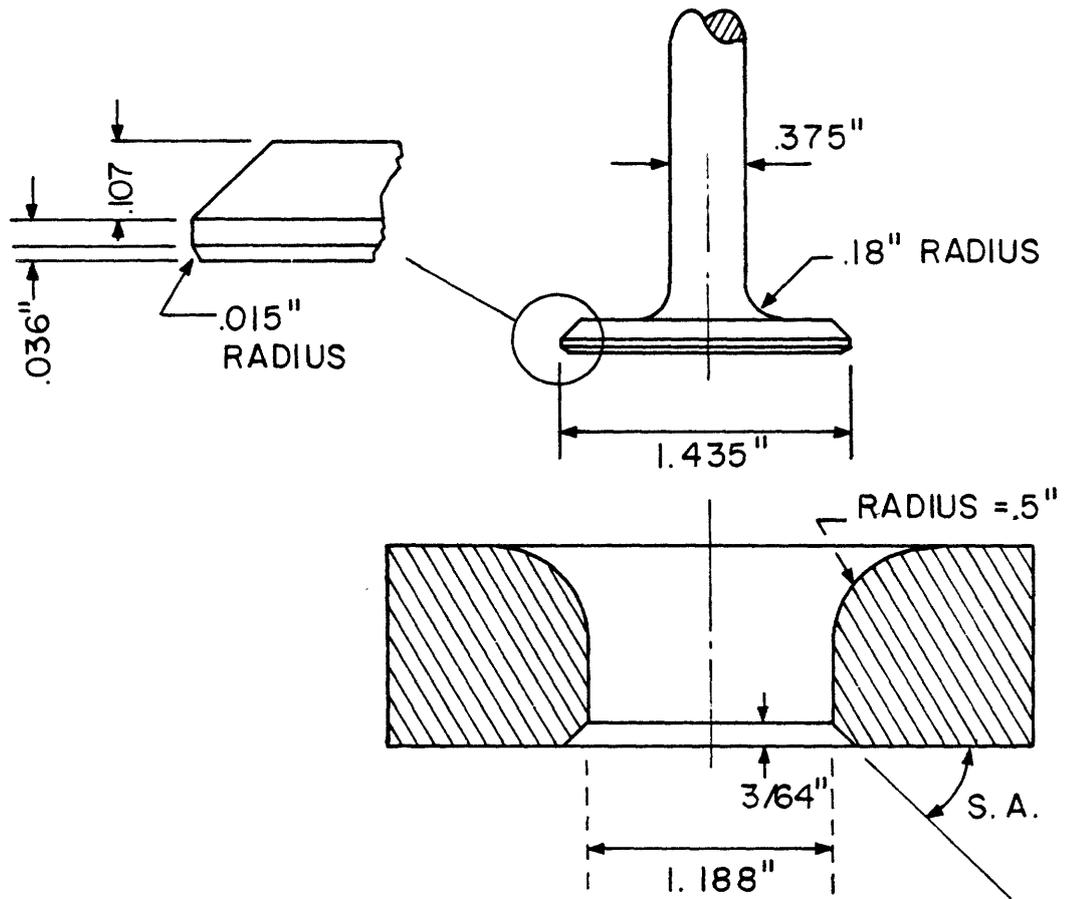
Fig. 2: Intake valve and seat geometry
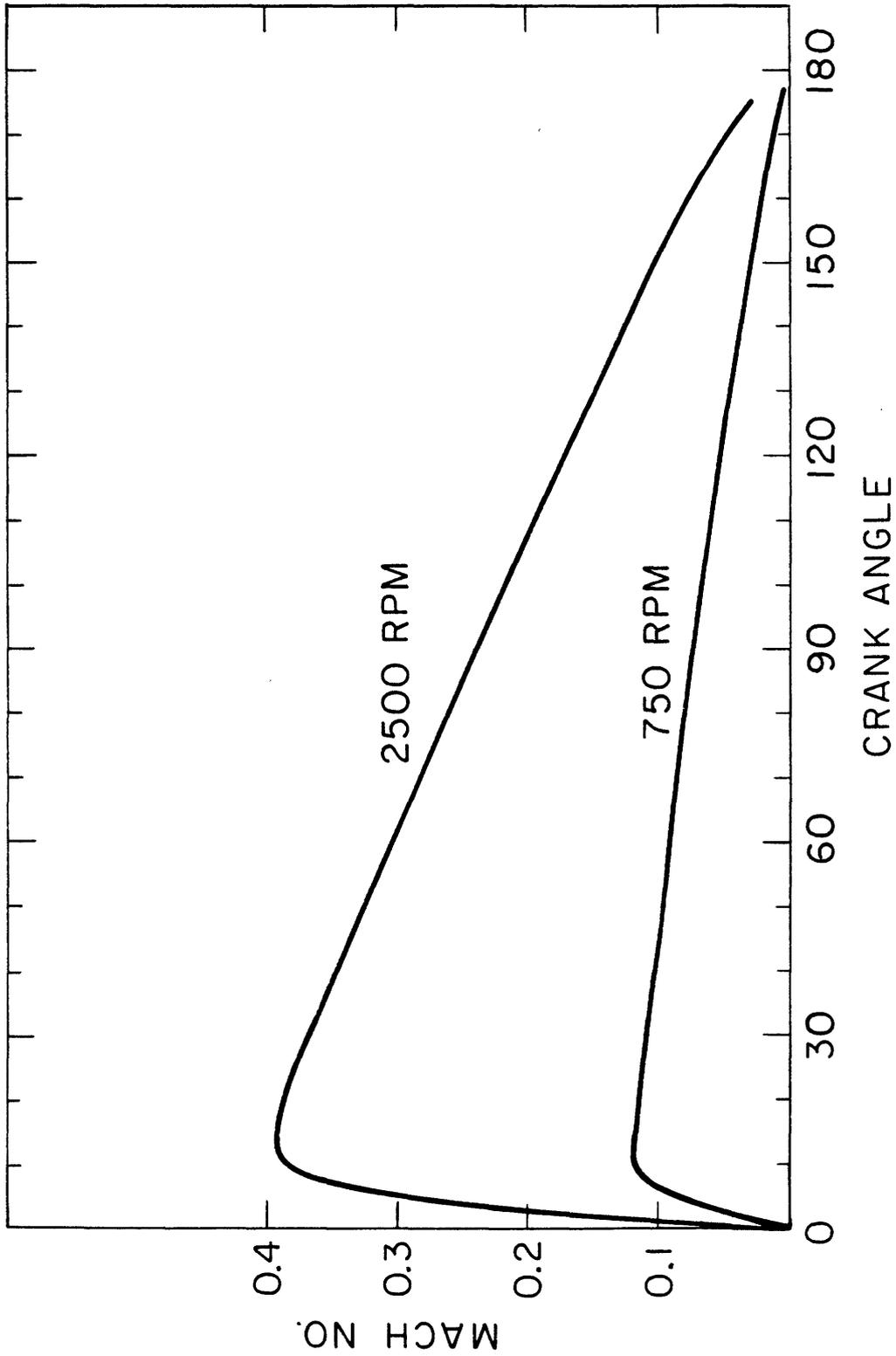
Fig. 3: Mach number at the valve throat during the intake process
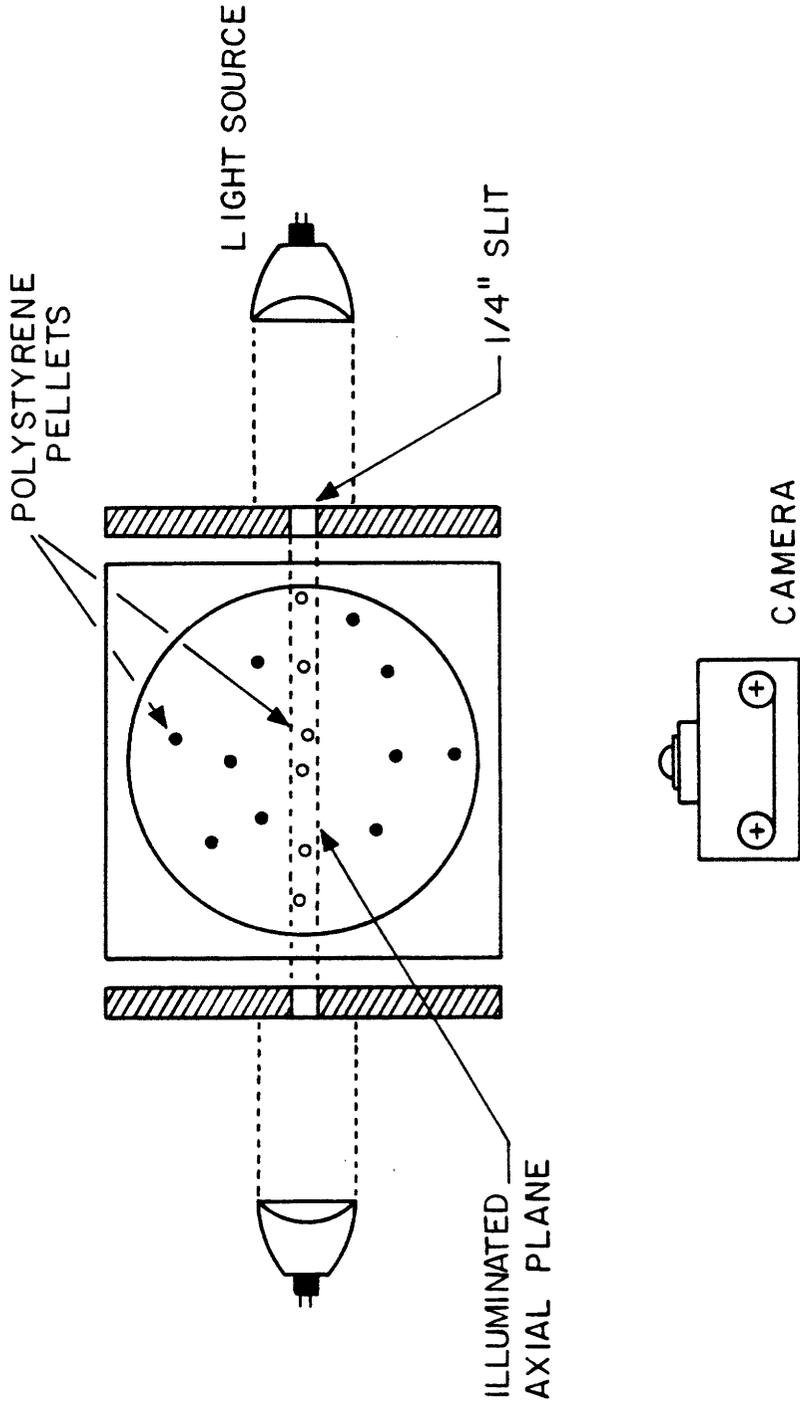
Fig. 4: Photography technique used with polystyrene tracers
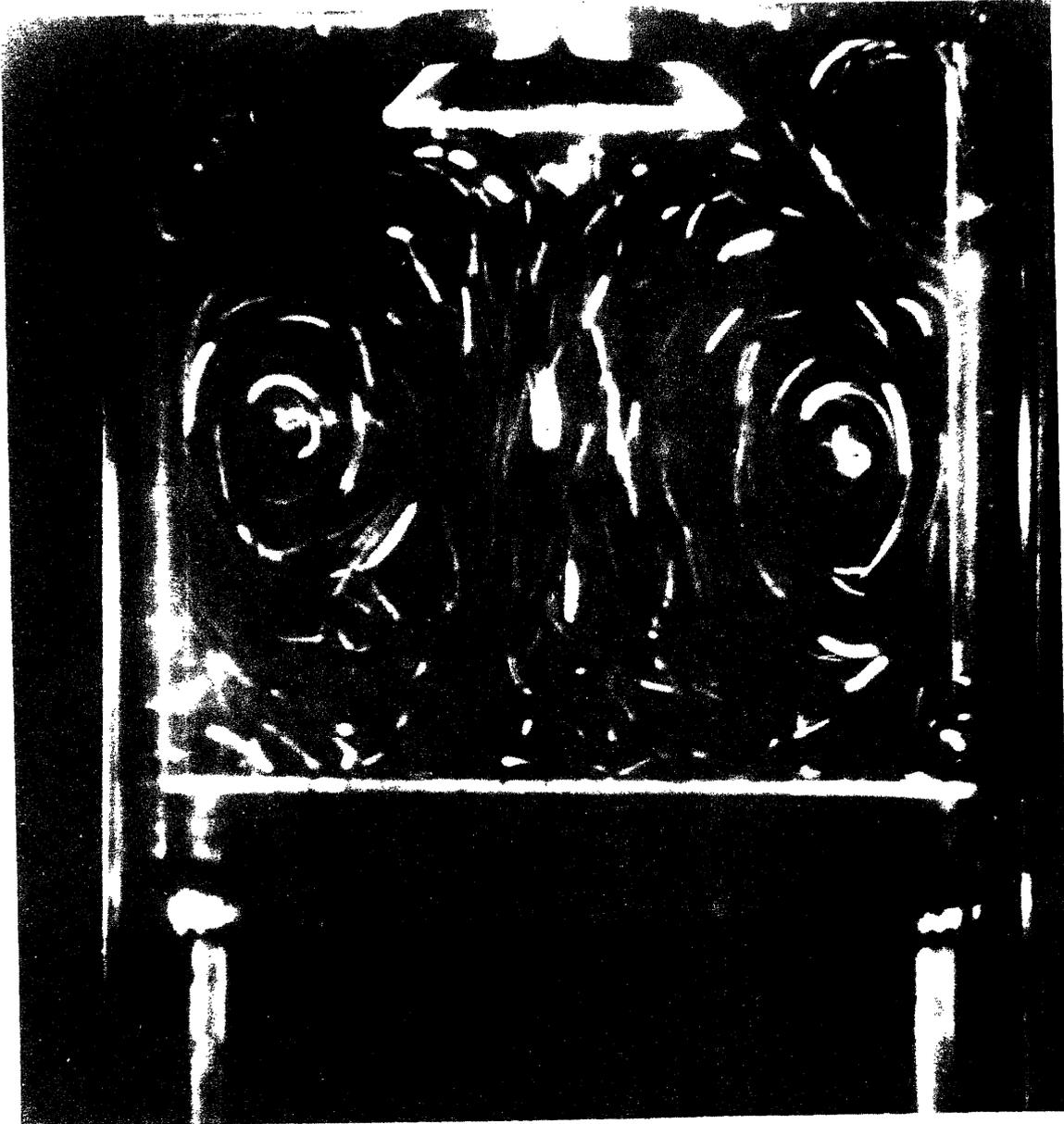
Fig. 5: Typical photograph of the structure of the flow during the intake process
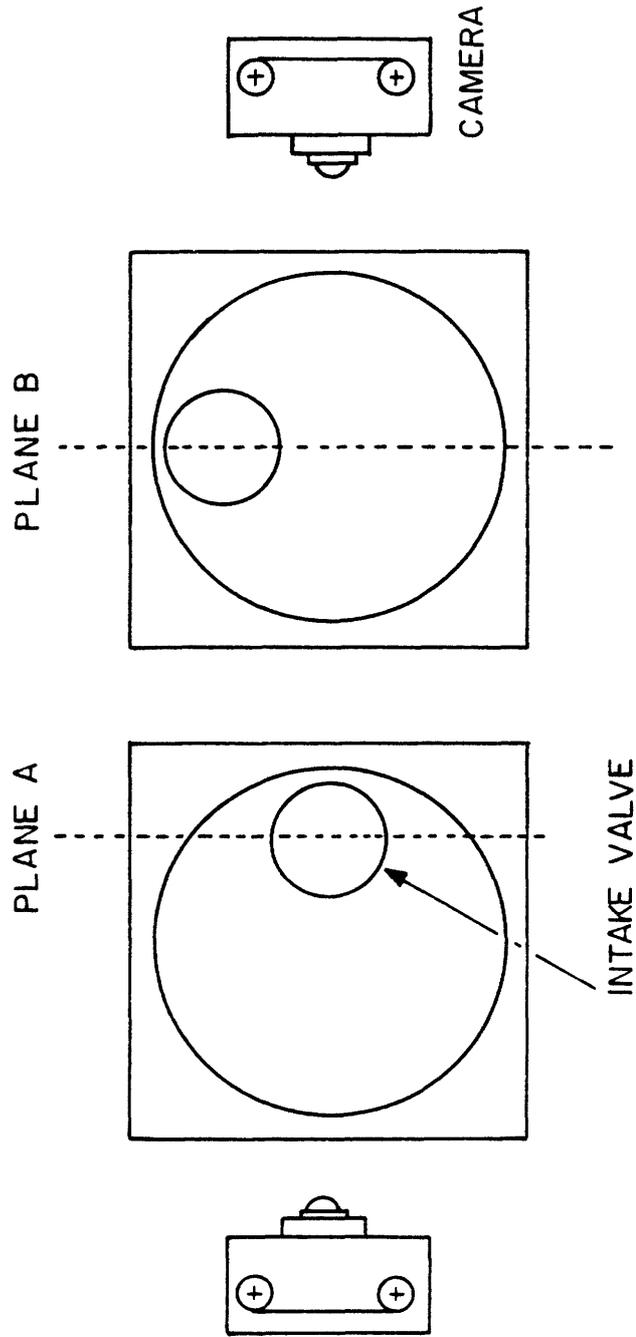
Fig. 6: Planes of the nonaxisymmetric geometry cylinder that were photographed
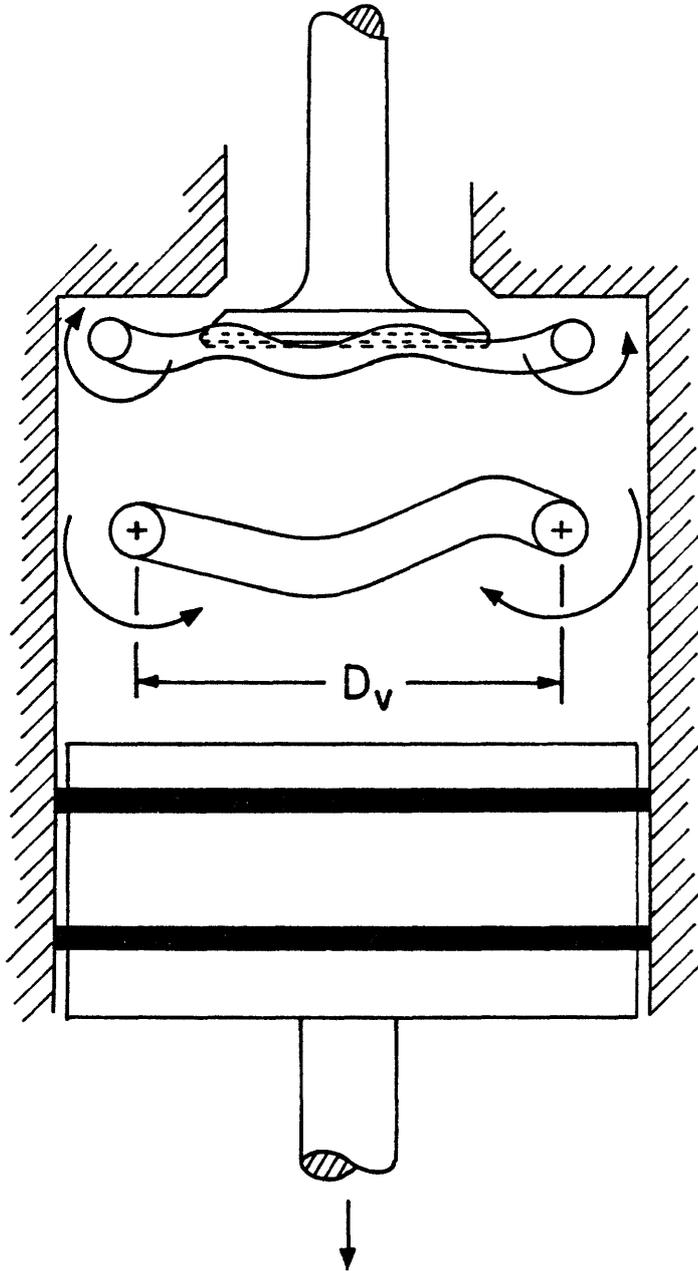
Fig. 7: Positions of the axes of rotation of the two
vortices for the axisymmetric case

B/S=1.35   LIFT=.21
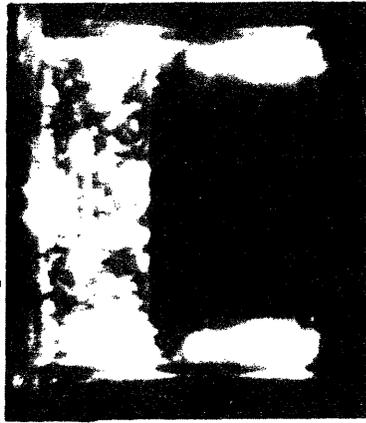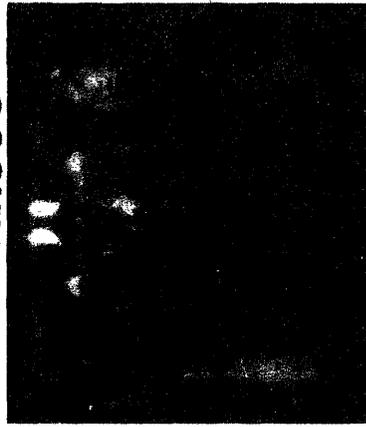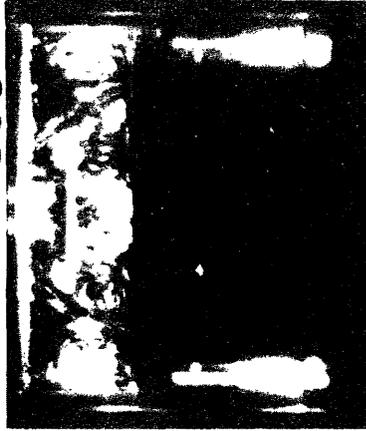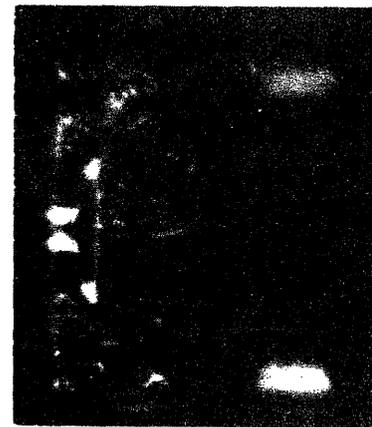
Fig. 8a: Effect of RPM on vortex structure; cases 1a, 2a and 3a

B/S=1.35   LIFT=.21

RPM=750   RPM=1500   RPM=2500
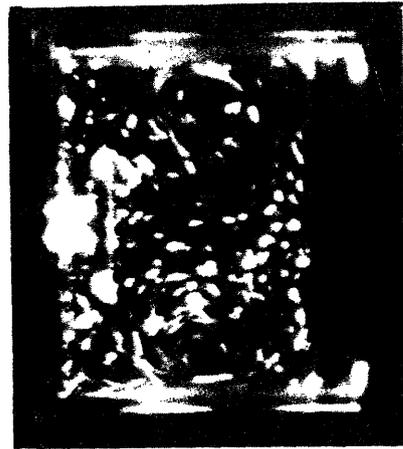
130°
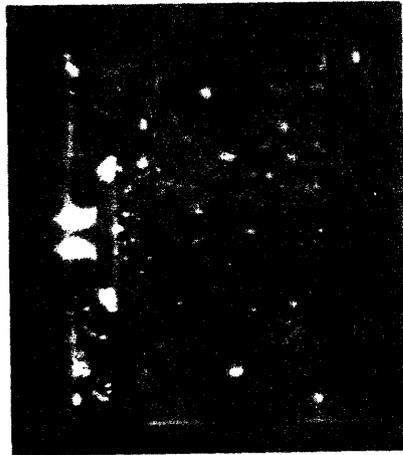
180°
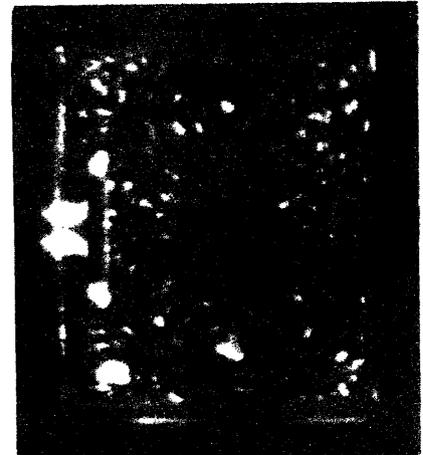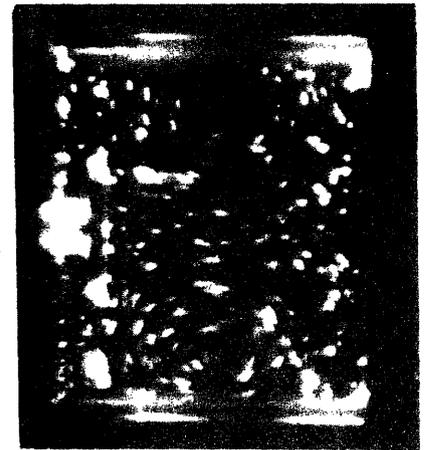
(Fig. 8b)
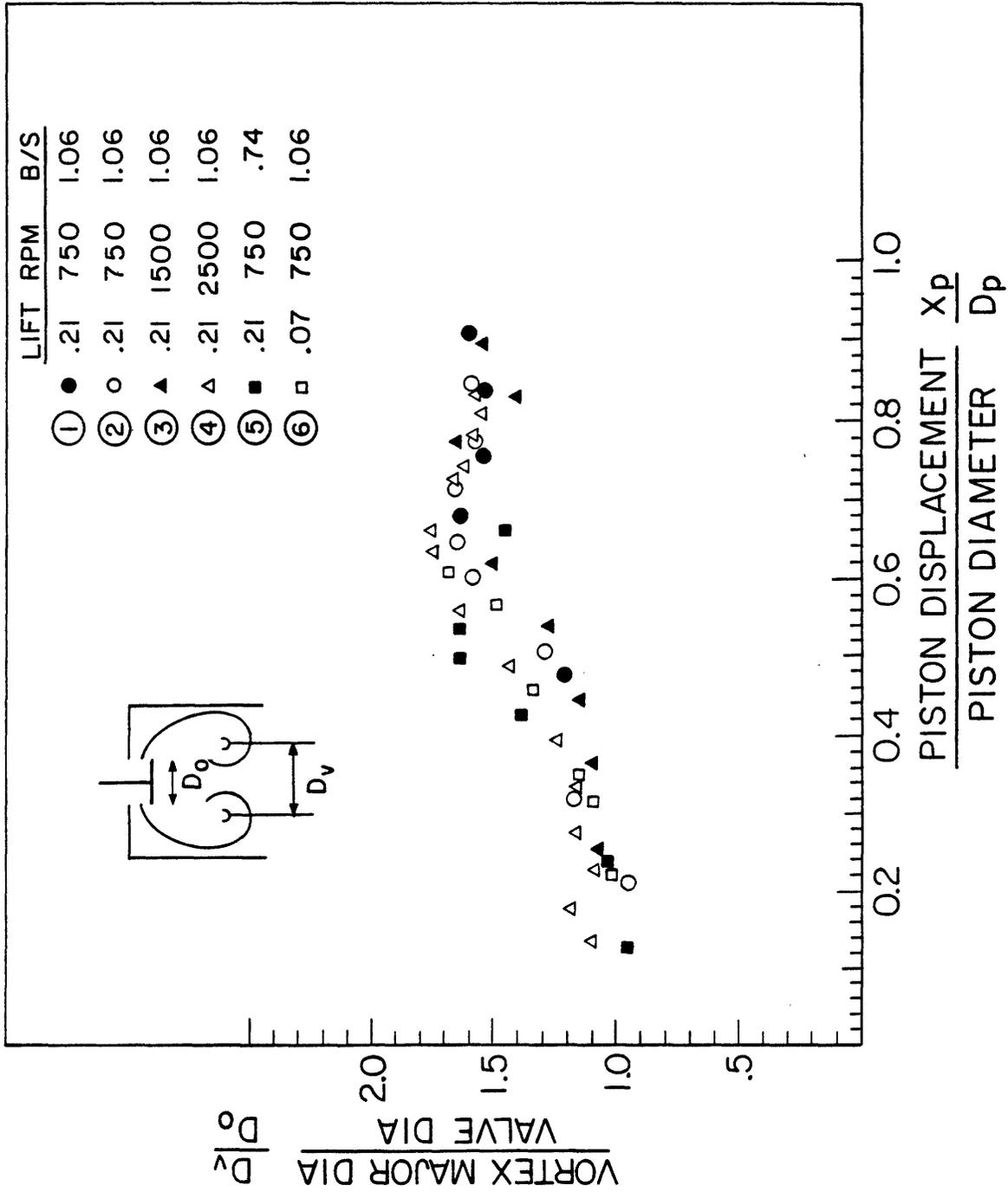
Fig. 9: Variation of dimensionless vortex major
diameter with dimensionless displacement
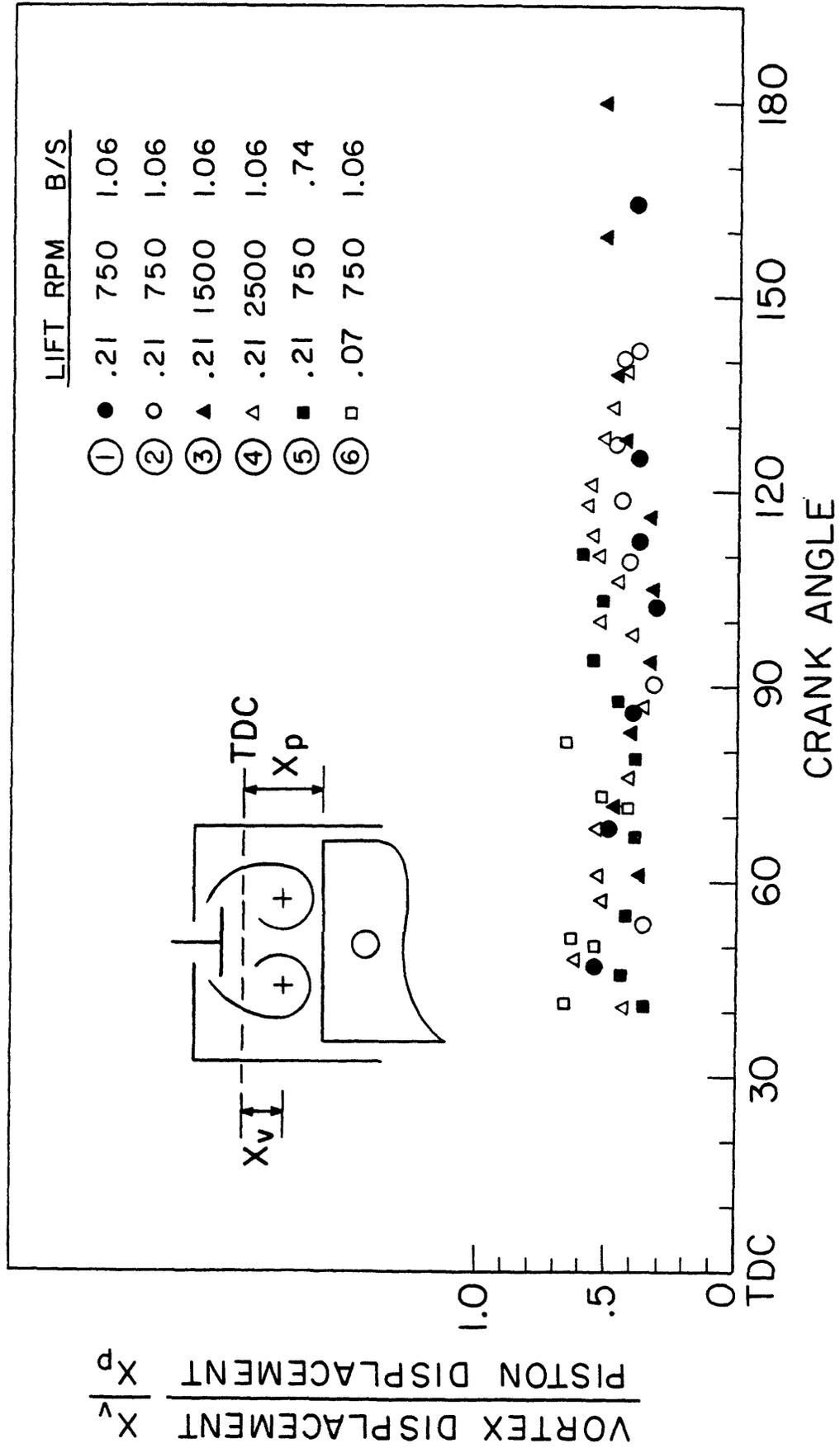
Fig. 10: Variation of vortex nondimensional position with crank angle
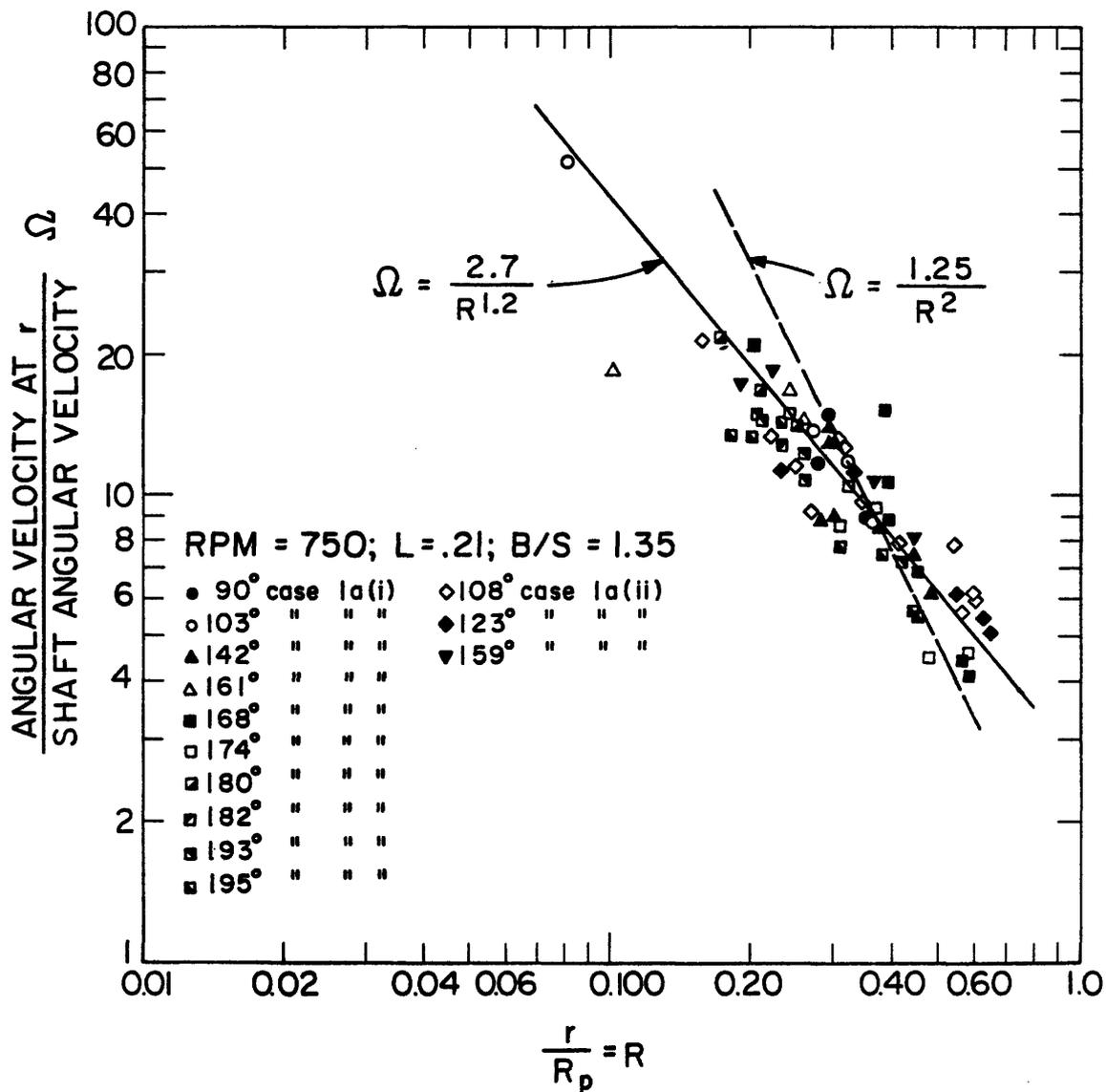
Fig. 11: Variation of nondimensional angular velocity in vortex with nondimensional radius, case 1a
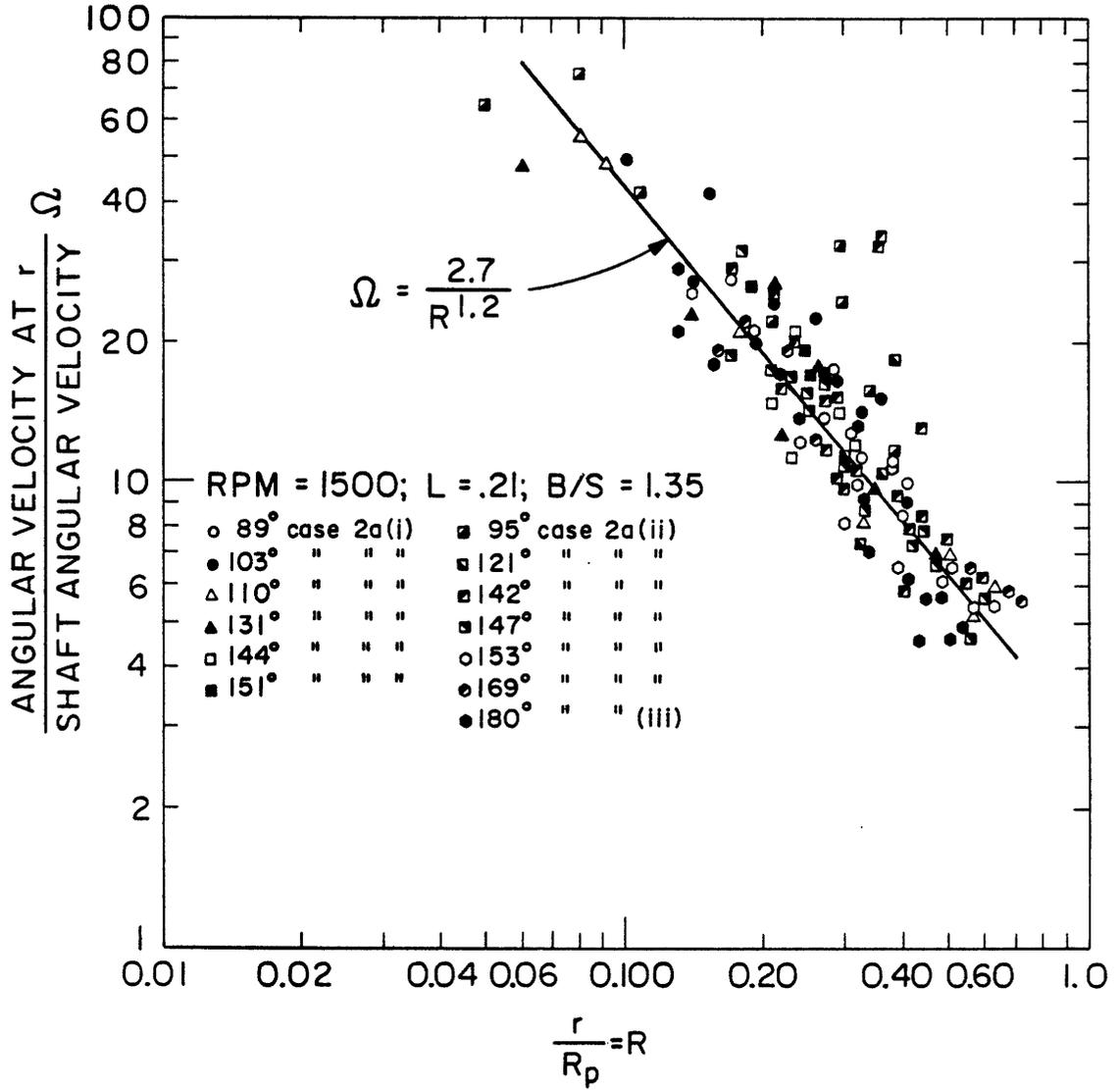
Fig. 12: Variation of nondimensional angular velocity in vortex with nondimensional radius, case 2a
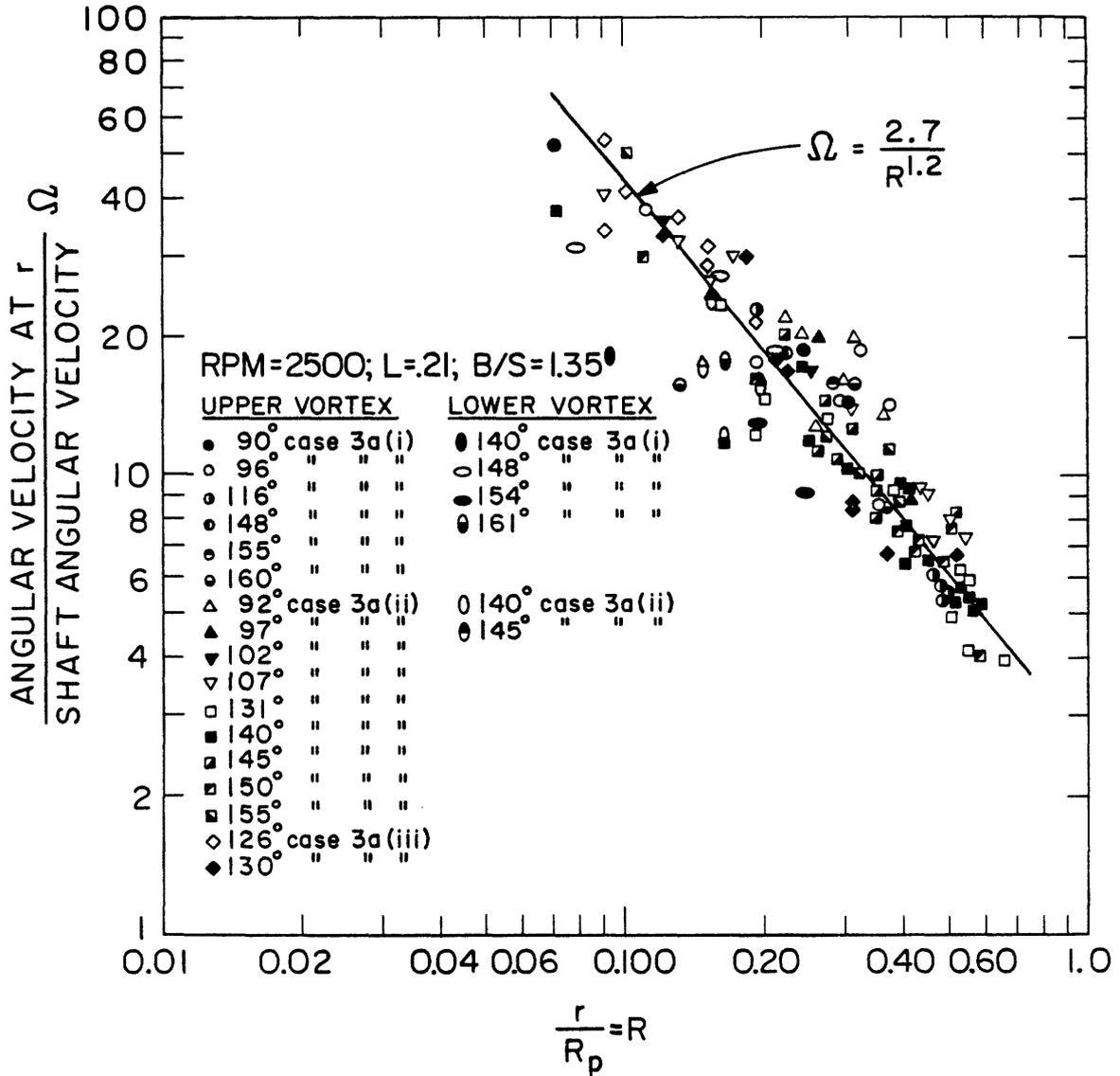
Fig. 13: Variation of nondimensional angular velocity
in vortex with nondimensional radius, case 3a
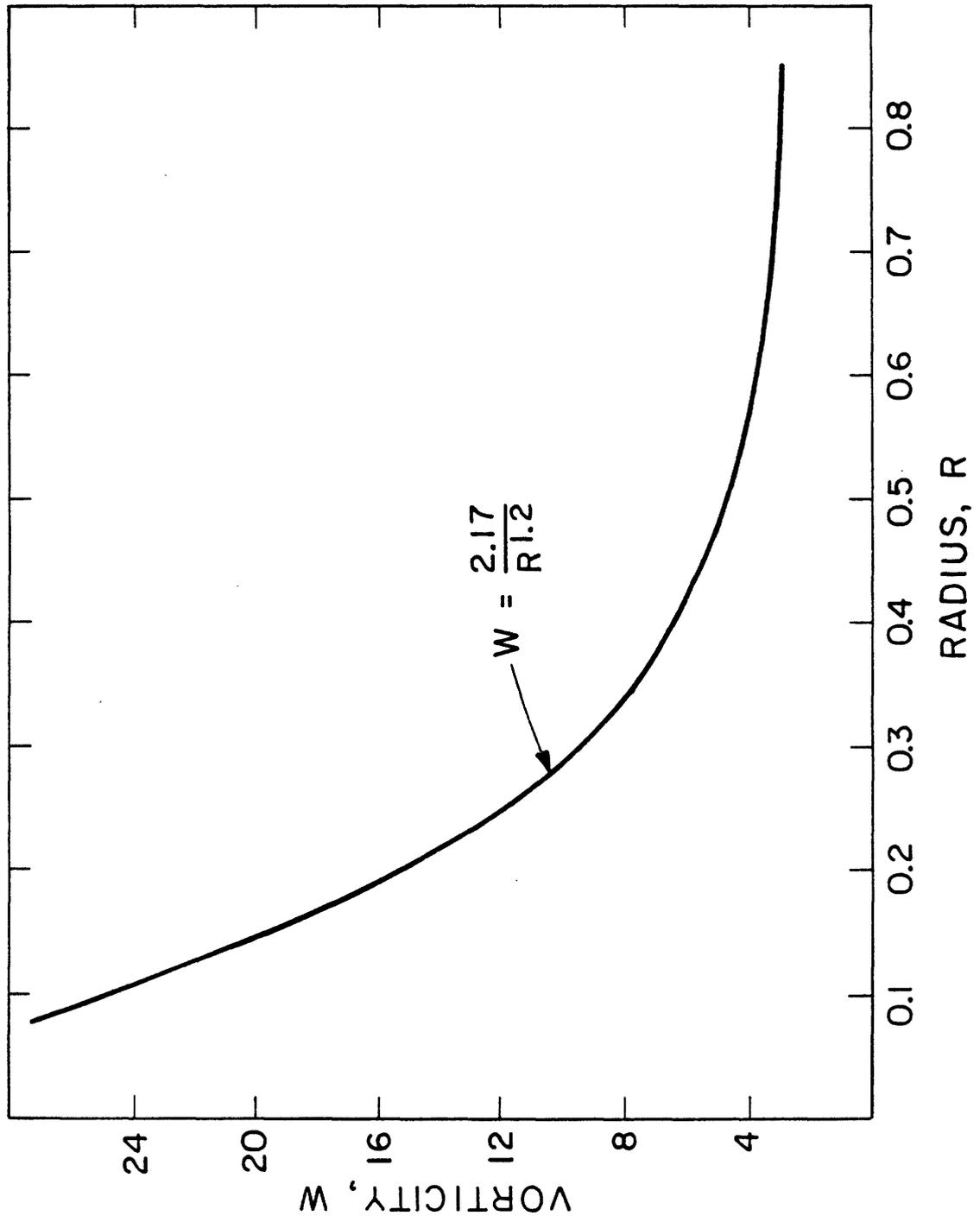
Fig. 14: Variation of nondimensional vorticity, W vs.
nondimensional radius, cases 1a, 2a and 3a

RPM = 750   LIFT = .21

B/S = .74   B/S = 1.06   B/S = 1.35
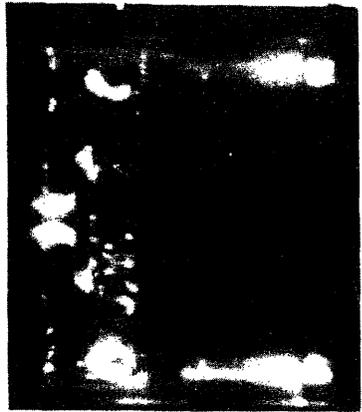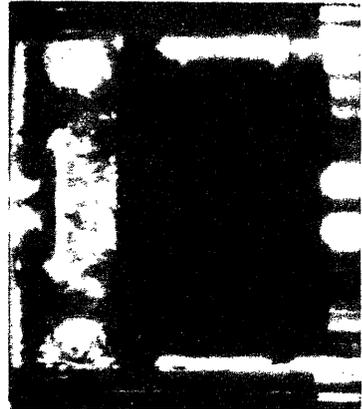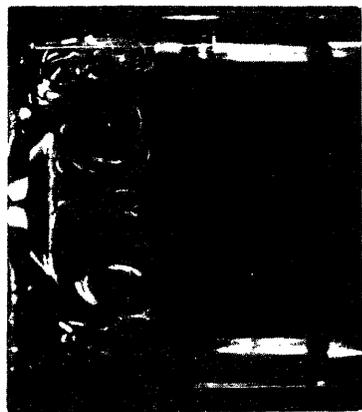
50°
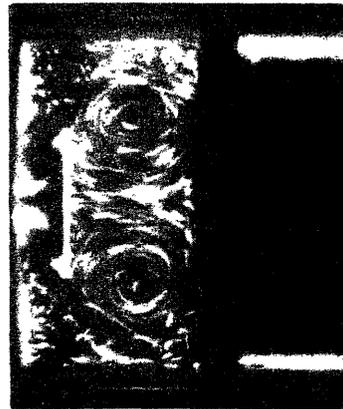
90°

Fig. 15a: Effect of length of stroke on vortex
structure; cases 4, 1b and 1a

RPM=750 LIFT=.21

B/S=.74 B/S=1.06 B/S=1.35
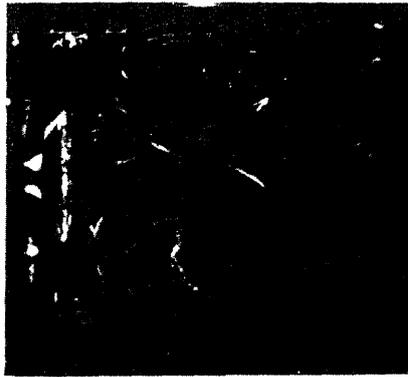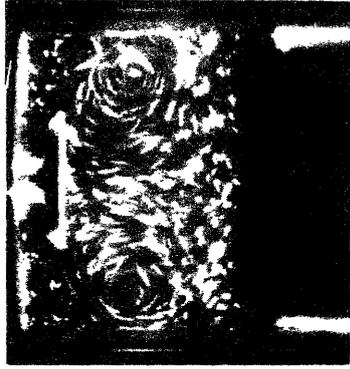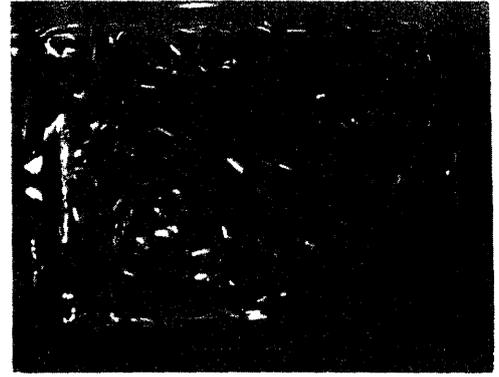
120° 180°
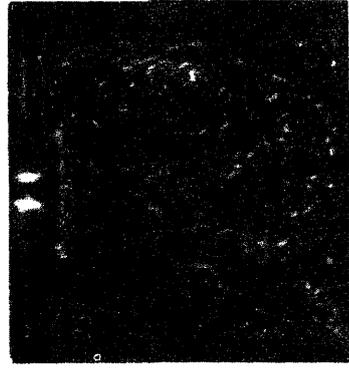
(Fig. 15b)

B/S=.74 RPM=345 LIFT=.07
(air bubble technique)
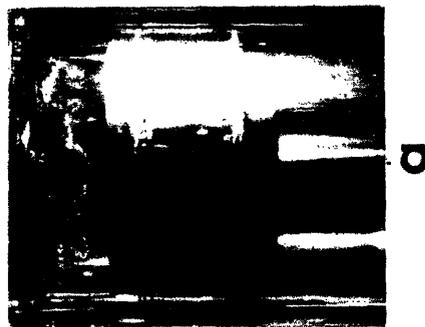
Fig. 16a: Axes of rotation visualized by air
bubbles; case 9

B/S=.74 RPM=345 LIFT=.07

e f

g h

(Fig. 16b)
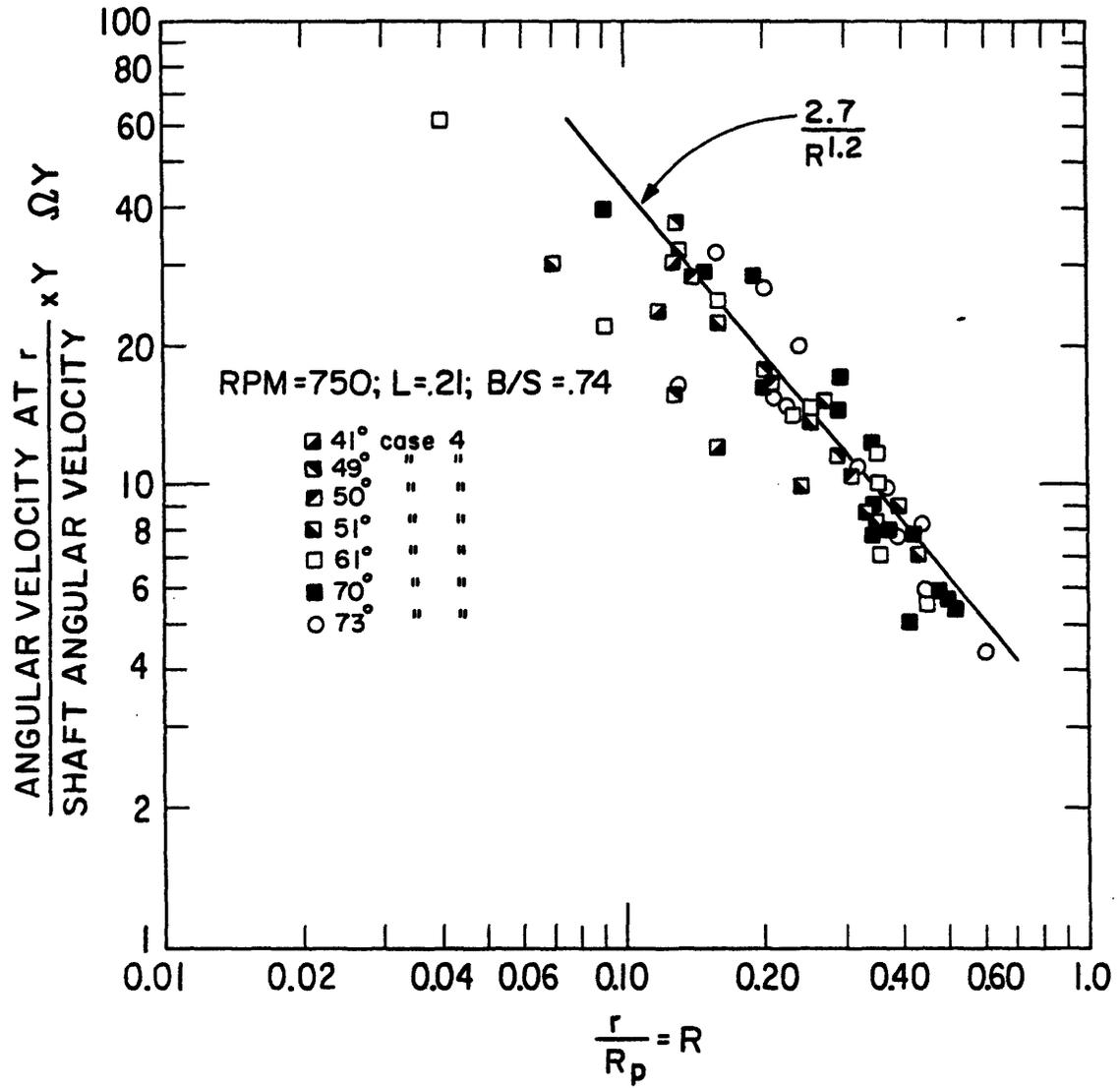
Fig. 17:   Variation of nondimensional angular velocity
with nondimensional radius, case 4
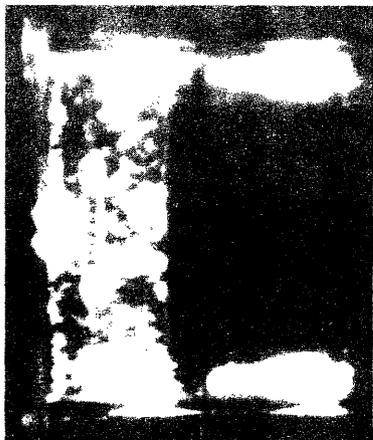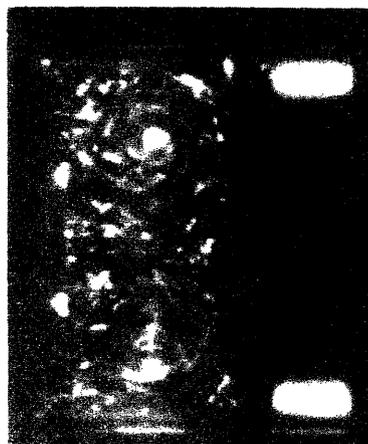
Fig. 18a: Effect of valve lift on vortex structure; cases 1a and 5

B/S=1.35 RPM=750

LIFT=.07

LIFT=.21

130°

180°
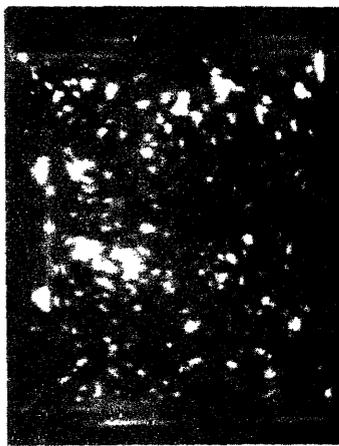
(Fig. 18b)
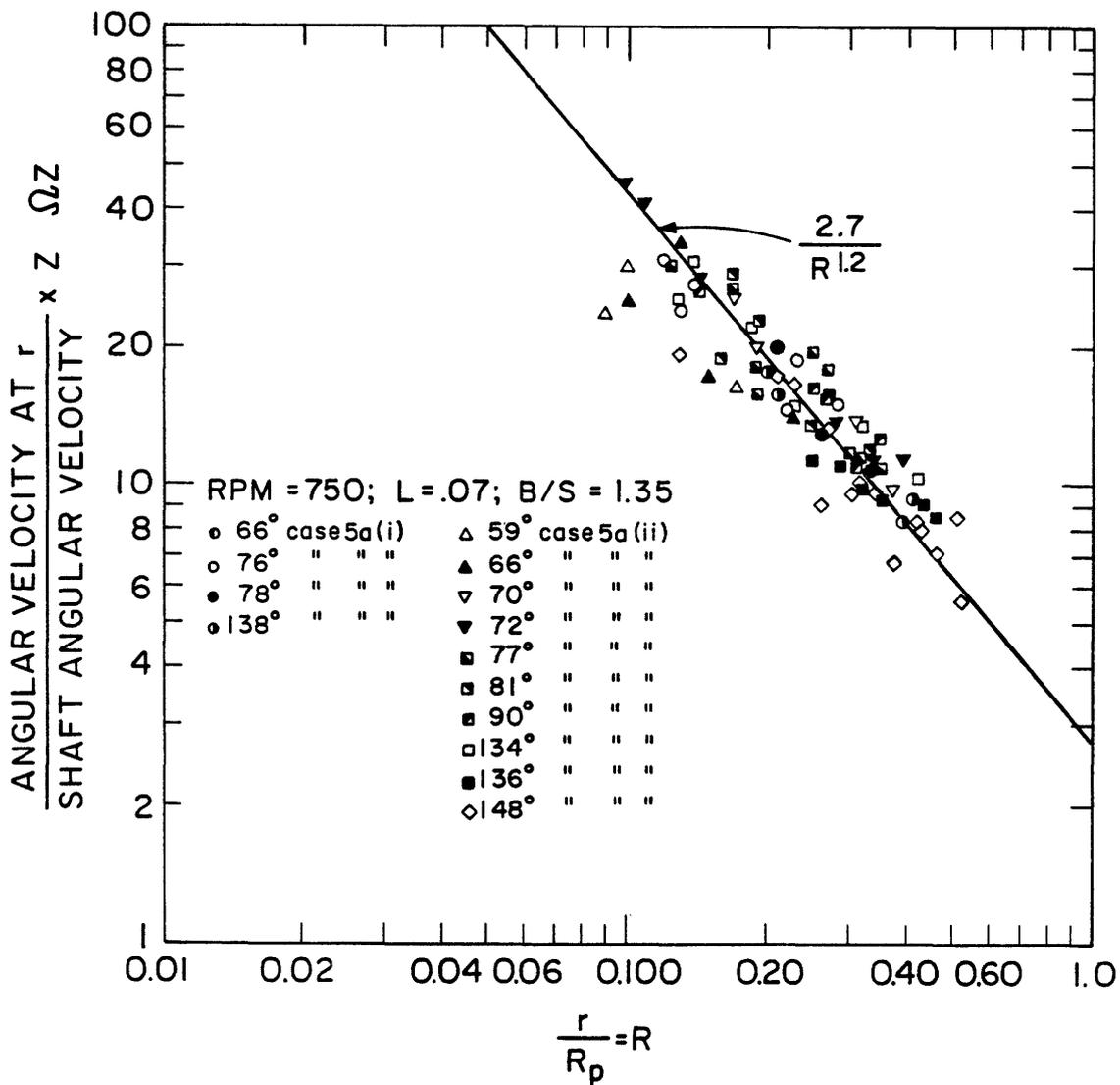
Fig. 19:   Variation of nondimensional angular velocity
           with nondimensional radius; case 5

B/S₌1.06

RPM₌750

S.A.₌30°   LIFT₌.07

S.A.₌30°   LIFT₌.21
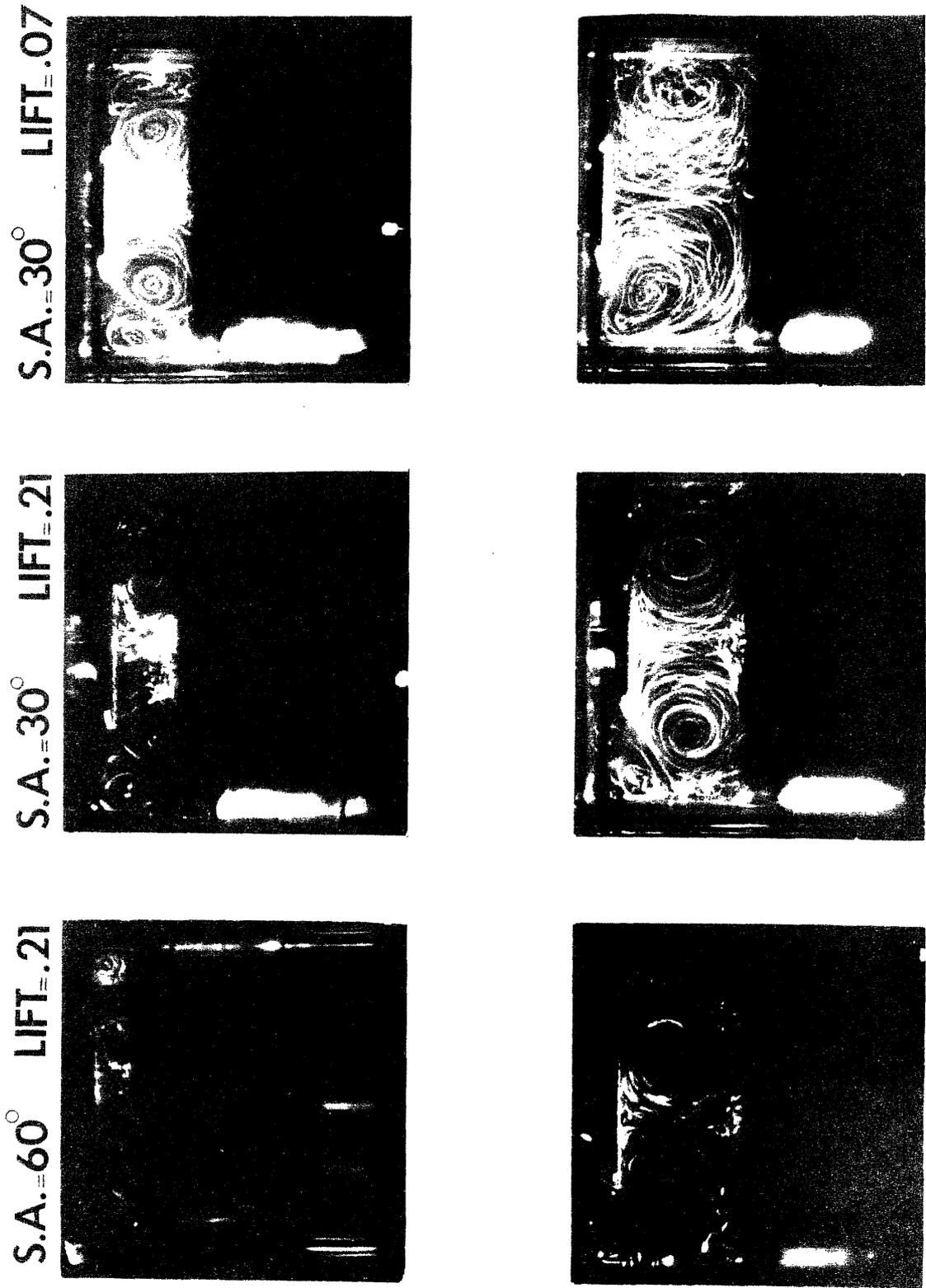
S.A.₌60°   LIFT₌.21

Fig. 20a: Effect of valve seat angle on flow field;
cases 6, 7a and 7b

RPM=750   B/S=1.06
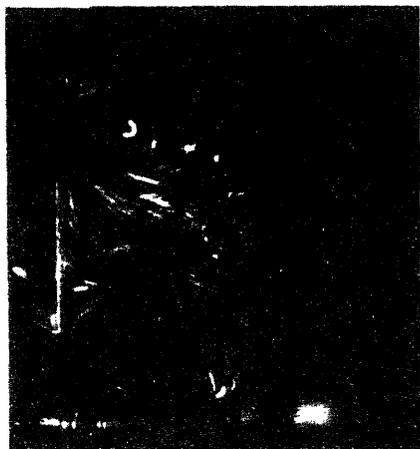
S.A.=60° LIFT=.21   S.A.=30° LIFT=.21   S.A.=30° LIFT=.07
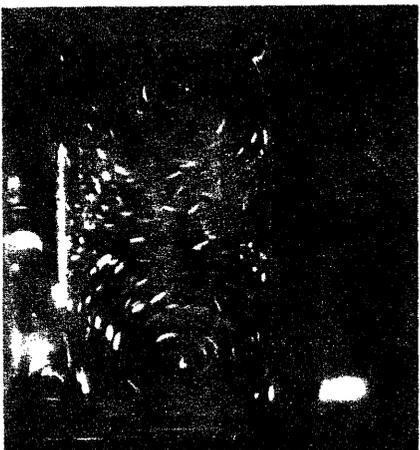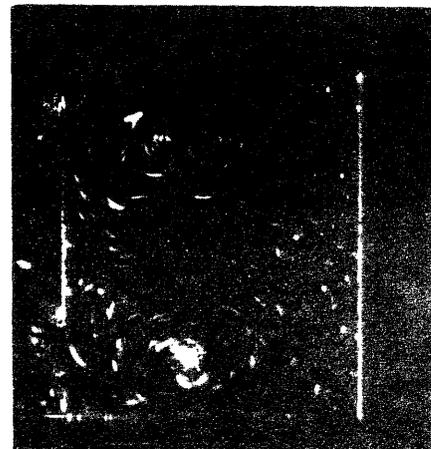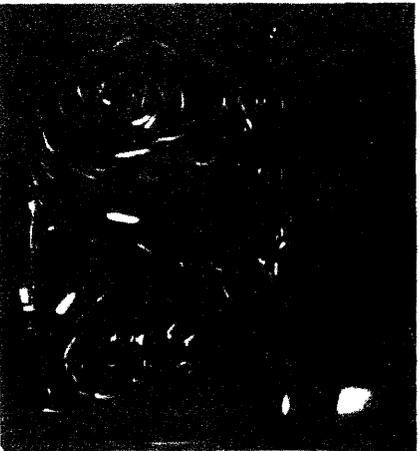
BDC

(Fig. 20b)

B/S=1.35 RPM=750 LIFT=.21

(off center valve)

.09

.06
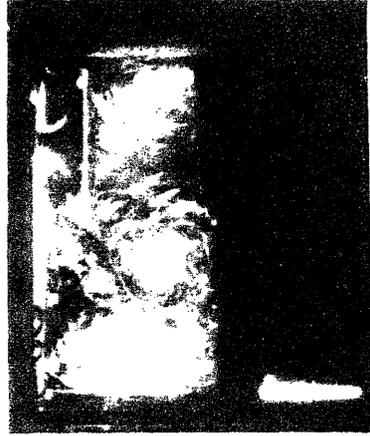
Fig. 21a: Vortex structure in nonaxisymmetric case;
plane A left column and plane B right
column (see Fig. 6)

B/S=1.35 R.P.M=750 LIFT=.21
(off center valve)
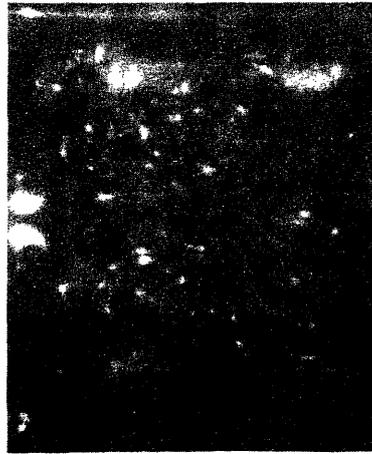
130°

180°

(Fig. 21b)

Fig. 22: Particle trajectories